Institute for Communications and Navigation

Code Bias and Multipath Estimation with Cascaded Kalman Filter

Mathieu Davaine

Institute for Communications and Navigation

Prof. Dr. Christoph Günther

Supervised by Patrick Henkel
Zhibo Wen

Munich, November, 2011

Institute for Communications and Navigation

Technische Universität München
Theresienstrasse 90
80333 Munich

Contents

Acknowledgements

I would like to thank Prof. Christoph Günther for his inspiring lecture in satellite navigation and for the opportunity to write my thesis at his institute.

My special thanks go to my supervisors Patrick Henkel and Zhibo Wen for their tremendous support, and numerous discussions even in the night.

I am also grateful to my girlfriend Caroline for her love, for her understanding and exceptional motivation.

I would also like to thank my parents Cristina and Thierry, who always wanted the best for me.

Chapter 1

Introduction

Precise Point Positioning (PPP) is becoming increasingly popular as it enables an absolute positioning with centimeter accuracy without the need of a reference station. However, the resolution of undifferenced carrier phase integer ambiguities requires precise knowledge of **satellite phase and code biases**.

Recently, *Laurichesse et al.*[1][2][3] have shown that fractional widelane biases can be assumed constant over several months and narrowlane biases are still constant on a daily basis, which enabled them to demonstrate undifferenced integer ambiguity resolution. They used a two stage procedure, i.e. they started with the geometry-free, ionosphere-free *Melbourne-Wübbena combination*[4], which provides the widelane integer ambiguities and a fractional bias, which is one of three correction parameters. Secondly, the widelane ambiguities are used as a priori knowledge in a Kalman filter, which processes ionosphere-free phase and ionosphere-free code combinations to estimate ionosphere-free phase clocks of both receivers and satellites, offsets between ionosphere-free phase and pseudorange clocks of both receivers and satellites, zenith tropospheric delays, station coordinate corrections, orbit corrections, and phase ambiguities. Laurichesse assumed a purely stochastic behavior for the ionosphere-free phase clocks, while a very tight model was used for the offset between ionosphere-free phase and pseudorange clocks (*1 cm process noise* for *station clocks*, *1 mm process noise* for *satellite clocks*). The ionosphere-free satellite phase clocks as well the offset between these phase and the respective pseudorange clocks set the second and third correction parameters for Laurichesse's precise point positioning.

In this thesis, satellite bias estimation is based on a much more general model, which does not use any linear combinations of measurements and, thus, benefits from less noisy measurements. The bias estimation is performed with a **Cascaded Kalman filter**. A first Kalman filter is used to estimate the geometry terms (in detail, only offsets w.r.t. a priori knowledge of ranges based on known ephemeris and station coordinates), the ionospheric delays, the integer phase ambiguities, and phase biases. A second Kalman filter is then used to refine the geometry term, i.e. it uses the a posteriori estimates of the first Kalman filter as measurements, and estimates orbital corrections, tropospheric zenith delays, satellite clock offsets (include code biases on one frequency), and receiver clock offsets (include code biases on one frequency). This approach has the advantage that it enables a *faster ambiguity resolution* compared to an estimation

of all unknowns in one single step. However, the first Kalman filter introduces a time correlation into the a posteriori estimates, such that the assumption of white Gaussian measurement noise is no longer fulfilled for the successive Kalman filter. Therefore, the method of *Bryson and Henrikson*[5] (1968) is applied. It first performs a time-differencing to whiten measurement errors. As this whitening introduces a correlation between measurement and process noises, a second decorrelation is performed to *decouple* the time-differenced measurement errors from the process errors. Both steps are combined in a generalized Kalman filter being used to determine orbital and clock corrections.

Besides the phase and code biases, **code multipath** is another major challenge for precise point positioning. Therefore, a time series of pseudorange residuals and its spectral transformation were analyzed for some IGS [6] stations in this thesis. A strong repeatability of multipath was observed over days, and a *sidereal filtering* was performed to obtain multipath corrections, which result in an almost white measurement noise.

Simulation results indicate that both the cascaded Kalman filter and code multipath corrections are two important steps to improve the reliability of precise point positioning.

Chapter 2

Laurichesse's Measurement Model

An accurate model of undifferenced code and carrier phase measurements is a crucial point. One option is to use individual clock/ bias parameters for each type of observation. Recently, Laurichesse et al. [3] re-parameterized the problem: They estimated individual clocks for the ionosphere-free phase and pseudorange combinations, and their offsets with respect to the clock offsets on L1. This parameterization has the advantage that it separates the stochastic parameters (ionosphere-free phase clock, ionosphere-free pseudorange clocks) from the clock parameters, that are only affected by longterm variations. Laurichesse's model lead to a very promising positioning performance, and is given by

$$\begin{aligned}
\rho_{i,1}^k &= g_{i,1}^k + c(\delta\tau_{\rho,i} - \delta\tau_\rho^k) + q_{11}^2 I_i^k + q_{11}^2(b_i - b^k) + \eta_{i,1}^k \\
\rho_{i,2}^k &= g_{i,2}^k + c(\delta\tau_{\rho,i} - \delta\tau_\rho^k) + q_{12}^2 I_i^k + q_{12}^2(b_i - b^k) + \eta_{i,2}^k \\
\lambda_1\varphi_{i,1}^k &= g_{i,1}^k + \lambda_1 W + c(\delta\tau_{\varphi,i} - \delta\tau_\varphi^k) - q_{11}^2 I_i^k - q_{11}^2(\beta_i - \beta^k) \\
&\quad +\lambda_1 N_{i,1}^k + \varepsilon_{i,1}^k \\
\lambda_2\varphi_{i,2}^k &= g_{i,2}^k + \lambda_2 W + c(\delta\tau_{\varphi,i} - \delta\tau_\varphi^k) - q_{12}^2 I_i^k - q_{12}^2(\beta_i - \beta^k) \\
&\quad +\lambda_2 N_{i,2}^k + \varepsilon_{i,2}^k,
\end{aligned} \tag{2.1}$$

with the following notations:

$g_{i,m}^k$	geometric propagation distance between the satellite and receiver antenna phase centers at frequency f_m including the tropospheric delay and relativistic effects
W	delay introduced by phase-wind up effect
$q_{1m} = \frac{f_1}{f_m}$	ratio between frequencies f_1 and f_m
I_i^k	slant ionospheric delay on frequency f_1
c	speed of light
$\delta\tau_{\rho,i}$	ionosphere-free pseudorange clock offset of receiver i
$\delta\tau_\rho^k$	ionosphere-free pseudorange clock offset of satellite k

$\delta\tau_{\varphi,i}$	ionosphere-free phase clock offset of receiver i
$\delta\tau_{\varphi}^{k}$	ionosphere-free phase clock offset of satellite k
b_i	difference between pseudorange clock offset on f_1 and ionosphere-free pseudorange clock offset for receiver i
b^k	difference between pseudorange clock offset on f_1 and ionosphere-free pseudorange clock offset for satellite k
β_i	difference between phase clock offset on f_1 and ionosphere-free phase clock offset for user i
β^k	difference between phase clock offset on f_1 and ionosphere-free phase clock offset for satellite k
$N_{i,m}^{k}$	carrier phase integer ambiguities.
$\eta_{i,m}^{k}$	pseudorange noise including multipath
$\varepsilon_{i,m}^{k}$	phase noise including multipath

An alternative parameterization to the use of separate phase and pseudorange clocks is the use of a common clock offset and individual biases for each type of observation as described in [7][8][9]. Setting the receiver clock offsets and biases of both models equal results in

$$\begin{aligned} c\delta\tau_{\rho,i} + q_{11}^2 b_i &= c\delta\tau_i + b_{i,1} \\ c\delta\tau_{\rho,i} + q_{12}^2 b_i &= c\delta\tau_i + b_{i,2} \\ c\delta\tau_{\phi,i} - q_{11}^2 \beta_i &= c\delta\tau_i + \beta_{i,1} \\ c\delta\tau_{\phi,i} - q_{12}^2 \beta_i &= c\delta\tau_i + \beta_{i,2}. \end{aligned} \tag{2.2}$$

This set of equations can also be written in matrix-vector-notation as

$$\underbrace{\begin{bmatrix} 1 & 0 & q_{11}^2 & 0 \\ 1 & 0 & q_{12}^2 & 0 \\ 0 & 1 & 0 & -q_{11}^2 \\ 0 & 1 & 0 & -q_{12}^2 \end{bmatrix}}_{\boldsymbol{A}} \begin{bmatrix} c\delta\tau_{\rho,i} \\ c\delta\tau_{\phi,i} \\ b_i \\ \beta_i \end{bmatrix} = \begin{bmatrix} c\delta\tau_i + b_{i,1} \\ c\delta\tau_i + b_{i,2} \\ c\delta\tau_i + \beta_{i,1} \\ c\delta\tau_i + \beta_{i,2} \end{bmatrix}, \tag{2.3}$$

which can be easily solved:

$$\begin{bmatrix} c\delta\tau_{\rho,i} \\ c\delta\tau_{\phi,i} \\ b_i \\ \beta_i \end{bmatrix} = \boldsymbol{A}^{-1} \begin{bmatrix} c\delta\tau_i + b_{i,1} \\ c\delta\tau_i + b_{i,2} \\ c\delta\tau_i + \beta_{i,1} \\ c\delta\tau_i + \beta_{i,2} \end{bmatrix}. \tag{2.4}$$

The estimation of ionosphere-free phase and pseudorange clocks is in general performed in two steps: in the first step, the geometry-free, ionosphere-free Melbourne-Wübbena code carrier linear combination is computed and averaged over time to obtain widelane integer ambiguities and fractional widelane biases. In the second step, the widelane ambiguity estimates are combined with the ionosphere-free phase-only linear combination to determine ionosphere-free phase and pseudorange clocks, code/ phase satellite/ receiver clock biases, satellite orbital corrections, tropospheric zenith delays and $N_{i,1}^{k}$ integer ambiguities in an extended Kalman filter.

The ionospheric delay I_u^k in the pseudorange measurements of (2.1) can be eliminated by a dual-frequency linear combination, i.e.

$$\rho_{i,\mathrm{IF}}^k = \alpha_1 \rho_{i,1}^k + \alpha_2 \rho_{i,2}^k, \tag{2.5}$$

where the two coefficients α_1 and α_2 are obtained from the geometry-preserving ($\alpha_1 + \alpha_2 = 1$) and ionosphere-free constraints ($\alpha_1 + \alpha_2 q_{12}^2 = 0$) as

$$\alpha_1 = \frac{q_{12}^2}{q_{12}^2 - 1} \quad \text{and} \quad \alpha_2 = -\frac{1}{q_{12}^2 - 1}. \tag{2.6}$$

The estimation of the ionosphere-free phase and pseudorange clocks requires a more precise model for the geometry term $g_{i,m}^k$, which is commonly modeled as

$$\begin{aligned} g_{i,m}^k &= \|\vec{\boldsymbol{x}}_i - \vec{\boldsymbol{x}}^k\| + d_m + m(\theta_i^k) T_{\mathrm{z}} \\ &= (\vec{\boldsymbol{e}}_i^k)^T (\vec{\boldsymbol{x}}_i - (\hat{\vec{\boldsymbol{x}}}^k + \delta\hat{\vec{\boldsymbol{x}}}^k)) + d_m + m(\theta_i^k) T_{\mathrm{z},i}, \end{aligned} \tag{2.7}$$

with the satellite position estimate $\hat{\vec{\boldsymbol{x}}}^k$ based on Keplerian orbit parameters, the satellite position error $\delta\hat{\vec{\boldsymbol{x}}}^k$, the difference d_m between the ionosphere-free phase center and the phase center on frequency f_m, and the slant tropospheric delay T_i^k, which is modeled as the product of an elevation-dependant mapping function $m(\theta_i^k)$, and a zenith delay $T_{\mathrm{z},i}$.

Thus, the ionosphere-free pseudorange and phase combinations can be obtained from (2.1), (2.5) and (2.7) as

$$\begin{aligned} \rho_{i,\mathrm{IF}}^k &= (\vec{\boldsymbol{e}}_i^k)^T (\vec{\boldsymbol{x}}_i - (\hat{\vec{\boldsymbol{x}}}^k + \delta\hat{\vec{\boldsymbol{x}}}^k)) + c(\delta\tau_{\rho,i} - \delta\tau_\rho^k) + m(\theta_i^k) T_{\mathrm{z}} + \eta_{i,\mathrm{IF}}^k \\ \lambda\varphi_{i,\mathrm{IF}}^k &= (\vec{\boldsymbol{e}}_i^k)^T (\vec{\boldsymbol{x}}_i - (\hat{\vec{\boldsymbol{x}}}^k + \delta\hat{\vec{\boldsymbol{x}}}^k)) + c(\delta\tau_{\varphi,i} - \delta\tau_\varphi^k) + m(\theta_i^k) T_{\mathrm{z}} + \frac{q_{12}^2 d_1 - d_2}{1 - q_{12}^2} \\ &\quad + \frac{q_{12}^2}{q_{12}^2 - 1} \lambda_1 N_{i,1}^k - \frac{1}{q_{12}^2 - 1} \lambda_2 N_{i,2}^k + \varepsilon_{i,\mathrm{IF}}^k. \end{aligned} \tag{2.8}$$

The ambiguity $N_{i,2}^k$ can be expressed as a function of $N_{i,1}^k$ and the a priori known widelane ambiguity $N_{\mathrm{WL}} = N_{i,1}^k - N_{i,2}^k$. The a priori known terms include the station coordinates $\vec{\boldsymbol{x}}_i$, the estimate of the satellite position $\hat{\vec{\boldsymbol{x}}}^k$, the linear combination of antenna phase center offsets $\frac{q_{12}^2 d_1 - d_2}{1 - q_{12}^2}$, and the widelane ambiguities N_{WL}, which are brought to the left sight of the equation:

$$\begin{aligned} \lambda\tilde{\varphi}_{i,\mathrm{IF}}^k &= \lambda\varphi_{i,\mathrm{IF}}^k - (\vec{\boldsymbol{e}}_i^k)^T (\vec{\boldsymbol{x}}_i - \hat{\vec{\boldsymbol{x}}}^k) - \frac{q_{12}^2 d_1 - d_2}{1 - q_{12}^2} - \frac{1}{q_{12}^2 - 1} \lambda_2 N_{\mathrm{WL}} \\ &= (\vec{\boldsymbol{e}}_i^k)^T \delta\vec{\boldsymbol{x}}^k + c(\delta\tau_{\varphi,i} - \delta\tau_\varphi^k) + m(\theta_i^k) T_{\mathrm{z}} + \underbrace{\frac{q_{12}^2 \lambda_1 - \lambda_2}{q_{12}^2 - 1}}_{\lambda_{\mathrm{NL}}} N_{i,1}^k + \varepsilon_{i,\mathrm{IF}}^k, \end{aligned} \tag{2.9}$$

with

$$\lambda_{\mathrm{NL}} = \frac{q_{12}^2 \lambda_1 - \lambda_2}{q_{12}^2 - 1} = \frac{f_1^2 \lambda_1 - f_2^2 \lambda_2}{f_1^2 - f_2^2} = c \cdot \frac{f_1 - f_2}{f_1^2 - f_2^2} = c \cdot \frac{1}{f_1 + f_2} = \frac{1}{\frac{1}{\lambda_1} + \frac{1}{\lambda_2}}, \tag{2.10}$$

which is 10.6 cm for dual frequency GPS measurements with $\lambda_1 = 19.0$ cm and $\lambda_2 = 24.4$ cm. The a priori known terms are also subtracted from the ionosphere-free pseudorange combination, i.e.

$$\tilde{\rho}^k_{i,\mathrm{IF}} = \rho^k_{i,\mathrm{IF}} - (\vec{\boldsymbol{e}}^k_i)^T(\vec{\boldsymbol{x}}_i - \hat{\vec{\boldsymbol{x}}}^k) = (\vec{\boldsymbol{e}}^k_i)^T\delta\vec{\boldsymbol{x}}^k + c(\delta\tau_{\rho,i} - \delta\tau^k_\rho) + m(\theta^k_i)T_\mathrm{z} + \eta^k_{i,\mathrm{IF}}. \tag{2.11}$$

Laurichesse used a Kalman filter to estimate orbital corrections $\delta\vec{\boldsymbol{x}}^k$, ionosphere-free phase clocks $c\delta\tau^k_\varphi$, and ionosphere-free pseudorange clocks $c\delta\tau^k_\rho$ from the linear combinations. As the Kalman filter will be introduced in a later section, only the process noise model and the obtained results for the offset between the ionosphere-free clocks and the clock offset on L1 shall be briefly introduced.

Table 2.1: Process noise model (Source: Laurichesse et al. [3])

Phase sat. clock	∞	purely stochastic
Phase rec. clock	∞	purely stochastic
Code/ phase sat. clock bias	1 mm	
Code/ phase rec. clock bias	1 cm	
Zenith tropospheric delay	1 mm	
Satellite orbit corrections	(0, 4 mm, 2 mm)	radial correction set to 0
Phase ambiguities	0	ambiguities are constant, initial covariance set to $100\mathrm{m}^2$

Laurichesse et al. [3] have processed phase and code measurements from 50 IGS stations to estimate the ionosphere-free phase clocks and the offsets between these ionosphere-free phase clocks and the ionosphere-free pseudorange clocks. Fig. 2.1 shows that long-term variations can be above one cycle, and tend to be larger for the older bloc IIA satellites compared to the bloc IIR satellites. However, the variations on a daily basis are negligible.

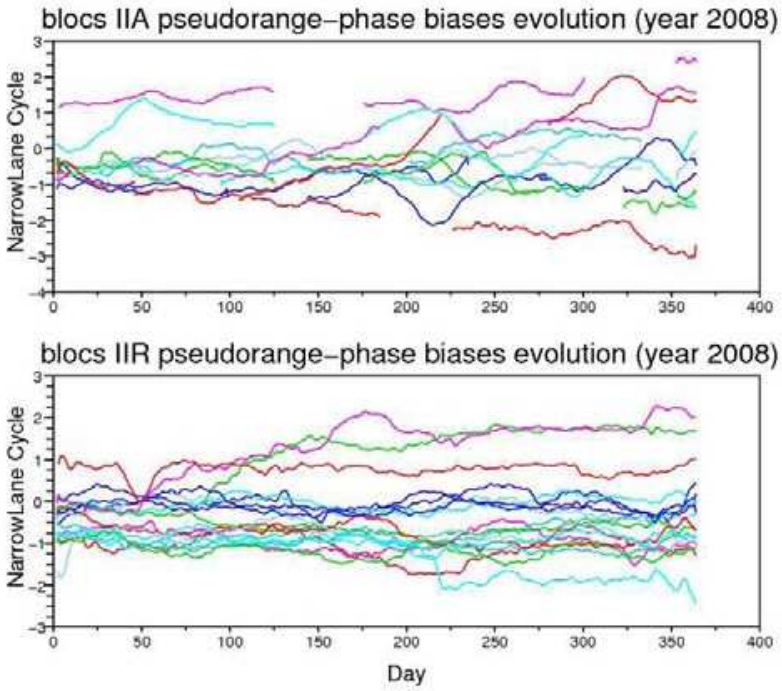

Figure 2.1: Evolution of pseudorange-phase biases over one year: This differential clock bias can be considered constant over one day but it shows long-term variations that can be far above one cycle. This motivates the estimation of individual phase clocks and pseudorange clocks. [3]

Chapter 3

Generalized Measurement Model

3.1 Model for undifferenced, uncombined Measurements

The most general model for undifferenced phase and code measurements at receiver i, from satellite k on frequency m was proposed by Günther in [10]:

$$\begin{aligned}
\lambda_1\phi^k_{1,i}(t_n) &= g^k_i(t_n) - I^k_{1,i}(t_n) + \lambda_1 N^k_{1,i} + \beta_{1,i} + \beta^k_1 + \epsilon^k_{1,i}(t_n) \\
\lambda_2\phi^k_{2,i}(t_n) &= g^k_i(t_n) - q^2_{12} I^k_{1,i}(t_n) + \lambda_2 N^k_{2,i} + \beta_{2,i} + \beta^k_2 + \epsilon^k_{2,i}(t_n) \\
\rho^k_{1,i}(t_n) &= g^k_i(t_n) + I^k_{1,i}(t_n) + b_{1,i} + b^k_1 + \eta^k_{1,i}(t_n) \\
\rho^k_{2,i}(t_n) &= g^k_i(t_n) + q^2_{12} I^k_{1,i}(t_n) + b_{2,i} + b^k_2 + \eta^k_{2,i}(t_n),
\end{aligned} \tag{3.1}$$

where:

λ_m	:	wavelength
$\phi^k_{m,i}$	:	carrier phase measurement
$\rho^k_{m,i}$	:	code measurement
t_n	:	epoch
g^k_i	:	geometry term
$I^k_{m,i}$	:	ionospheric slant delay
$N^k_{m,i}$	:	integer ambiguity
$\beta_{m,i}$	:	receiver phase bias
β^k_m	:	satellite phase bias
$b_{m,i}$	:	receiver code bias
b^k_m	:	satellite code bias
$\epsilon^k_{m,i}$	:	phase noise
$\eta^k_{m,i}$	:	code noise,

and $q_{12} = f_1/f_2$ denotes the frequency ratio.

The geometry term contains all non-dispersive terms and is described by:

$$g^k_i(t_n) = r^k_i(t_n) + c(\delta\tau_i(t_n) - \delta\tau^k(t_n - \Delta\tau^k_i(t_n))) + T^k_i(t_n), \tag{3.2}$$

with

$$r_i^k(t_n) = \left\| \vec{r}_i - \vec{r}^k(t_n - \Delta\tau_i^k(t_n)) \right\|, \tag{3.3}$$

where r_i^k denotes the range between receiver i and satellite k, $\delta\tau_i$ and $\delta\tau^k$ denote the receiver and satellite clock offsets and T_i^k denotes the tropospheric delay. $\Delta\tau_i^k(t_n)$ describes the propagation time of the signal from the satellite to the receiver at the reception time t_n, i.e. the difference in time between signal emission and reception.

A dynamic model of second order is introduced for the geometry term g_i^k:

$$g_i^k(t_n) = g_i^k(t_{n-1}) + \Delta t \dot{g}_i^k(t_{n-1}) + \frac{1}{2}\Delta t^2 \ddot{g}_i^k(t_{n-1}) + w_{g_i^k}(t_n), \tag{3.4}$$

where $w_{g_i^k}(t_n)$ denotes the process noise.

The ionospheric slant delay is assumed to be a Gauss-Markov process, allowing the accumulation of white Gaussian noise, i.e.

$$I_{1,i}^k(t_n) = I_{1,i}^k(t_{n-1}) + w_{I_i^k}(t_n), \tag{3.5}$$

with $w_{I_i^k} \sim \mathcal{N}(0, \sigma^2_{w_{I_i^k}})$.

3.2 Parameter Mapping

The estimation of all the parameters in (3.1) is not possible due to the rank deficiency of the system of equations. Assuming

$$N_{\text{MEAS}} = \sum_{i=1}^{R} K_i, \tag{3.6}$$

with R denoting the total number of receivers and K_i being the number of visible satellites to receiver i, the model provides $4N_{\text{MEAS}}$ measurements (code and phase measurements for each satellite/receiver pair on 2 frequencies). However the number of unknowns is obtained from

$$\begin{aligned} N_{\text{UNKNOWN}} &= N_{g_i^k} + N_{I_{1,i}^k} + N_{N_{m,i}^k} + N_{\beta_{m,i}} + N_{\beta_m^k} + N_{b_{m,i}} + N_{b_m^k} \\ &= N_{\text{MEAS}} + N_{\text{MEAS}} + 2N_{\text{MEAS}} + 2R + 2K + 2R + 2K \\ &= 4N_{\text{MEAS}} + 4(K+R) > 4KR, \end{aligned} \tag{3.7}$$

which means the current system has $4(K+R)$ more unknowns than measurements. Thus, the system of Eq.(3.1) is singular. In order to solve the system of equations, a set of mappings [8][7] is applied to the unknowns to remove the rank deficiency, i.e. new unknowns are created by performing linear combinations of previous ones.

In a first step, code biases are mapped into the geometry and ionospheric terms:

$$\tilde{g}_i^k(t_n) = g_i^k(t_n) + b_{g_i} + b_{g^k} \tag{3.8}$$

$$\tilde{I}_{1,i}^k(t_n) = I_{1,i}^k(t_n) + b_{I_i} + b_{I^k}, \tag{3.9}$$

with

$$b_{g_i} = -\frac{b_{2,i} - q_{12}^2 b_{1,i}}{q_{12}^2 - 1} \tag{3.10}$$

$$b_{g^k} = -\frac{b_2^k - q_{12}^2 b_1^k}{q_{12}^2 - 1} \tag{3.11}$$

$$b_{I_i} = \frac{b_{1,i} - b_{2,i}}{q_{12}^2 - 1} \tag{3.12}$$

$$b_{I^k} = \frac{b_1^k - b_2^k}{q_{12}^2 - 1}. \tag{3.13}$$

Since the geometry and ionospheric terms also appear in the phase measurements, the phase bias terms are affected accordingly:

$$\tilde{\beta}_{1,i} = \beta_{1,i} - b_{g_i} + b_{I_i} \tag{3.14}$$

$$\tilde{\beta}_{2,i} = \beta_{2,i} - b_{g_i} + q_{12}^2 b_{I_i} \tag{3.15}$$

$$\tilde{\beta}_1^k = \beta_1^k - b_{g^k} + b_{I^k} \tag{3.16}$$

$$\tilde{\beta}_2^k = \beta_2^k - b_{g^k} + q_{12}^2 b_{I^k}. \tag{3.17}$$

This first mapping reduces the number of unknowns from $4N_{\text{MEAS}}+4(R+K)$ (3.7) to $4N_{\text{MEAS}} + 2(R + K)$.

In the second step, one satellite is chosen as reference. Its corresponding phase biases on each frequency are mapped to the other satellite phase biases and are compensated in the receiver phase biases, i.e.

$$\tilde{\tilde{\beta}}_1^k = \tilde{\beta}_1^k - \tilde{\beta}_1^1 \tag{3.18}$$

$$\tilde{\tilde{\beta}}_2^k = \tilde{\beta}_2^k - \tilde{\beta}_2^1 \tag{3.19}$$

$$\tilde{\tilde{\beta}}_{m,1} = \tilde{\beta}_{1,i} + \tilde{\beta}_1^1 \tag{3.20}$$

$$\tilde{\tilde{\beta}}_{m,2} = \tilde{\beta}_{2,i} + \tilde{\beta}_2^1, \tag{3.21}$$

which allows a reduction to $4N_{\text{MEAS}} + 2(R + K - 1)$ unknowns. To get rid of the remaining dependencies, a third mapping is performed on the ambiguities [11]. The main idea is to map a subset of $2(R + K - 1)$ ambiguities to other ambiguities and phase biases through Gaussian elimination.

$$\tilde{\tilde{\beta}}_i = \tilde{\tilde{\beta}}_i + \sum_{N_j \in N_{\text{sub}}} c_{j,i} N_j \tag{3.22}$$

$$\tilde{\tilde{\beta}}^k = \tilde{\tilde{\beta}}^k + \sum_{N_j \in N_{\text{sub}}} c_j^k N_j \tag{3.23}$$

$$\tilde{N}_i^k = N_i^k + \sum_{N_j \in N_{\text{sub}}} c_{j,i}^k N_j, \tag{3.24}$$

where the subset is denoted by N_{sub} and $c_{j,i}$, c_j^k and $c_{j,i}^k$ denote the coefficients generated by Gaussian elimination.

The measurement model after the set of parameter mappings is written as:

$$\begin{aligned}
\lambda_1\phi_{1,i}^k(t_n) &= \tilde{g}_i^k(t_n) - \tilde{I}_{1,i}^k(t_n) + \lambda_1\tilde{N}_{1,i}^k + \tilde{\tilde{\beta}}_{1,i} + \tilde{\tilde{\beta}}_1^k + \epsilon_{1,i}^k(t_n) \\
\lambda_2\phi_{2,i}^k(t_n) &= \tilde{g}_i^k(t_n) - q_{12}^2\tilde{I}_{1,i}^k(t_n) + \lambda_2\tilde{N}_{2,i}^k + \tilde{\tilde{\beta}}_{2,i} + \tilde{\tilde{\beta}}_2^k + \epsilon_{2,i}^k(t_n) \\
\rho_{1,i}^k(t_n) &= \tilde{g}_i^k(t_n) + \tilde{I}_{1,i}^k(t_n) + \eta_{1,i}^k(t_n) \\
\rho_{2,i}^k(t_n) &= \tilde{g}_i^k(t_n) + q_{12}^2\tilde{I}_{1,i}^k(t_n) + \eta_{2,i}^k(t_n).
\end{aligned} \tag{3.25}$$

3.3 A Priori Information: Widelane Double Difference Integer Ambiguities

The widelane Melbourne-Wübbena combination W_i^k is defined as:

$$W_i^k = \left(\frac{f_1}{f_1 - f_2}\lambda_1\phi_{1,i}^k - \frac{f_2}{f_1 - f_2}\lambda_2\phi_{2,i}^k\right) - \left(\frac{f_1}{f_1 + f_2}\rho_{1,i}^k + \frac{f_2}{f_1 + f_2}\rho_{2,i}^k\right), \tag{3.26}$$

which is geometry-free and ionosphere-free, i.e.

$$\begin{aligned}
W_i^k = &\left(g_i^k + \frac{1}{f_1 - f_2}\left(-f_1 I_{1,i}^k + f_2 q_{12}^2 I_{1,i}^k\right.\right. \\
&\left.\left. + f_1\left(\lambda_1 N_{1,i}^k + \beta_1^k + \epsilon_{1,i}^k\right) - f_2\left(\lambda_2 N_{2,i}^k + \beta_2^k + \epsilon_{2,i}^k\right)\right)\right) \\
&- \left(g_i^k + \frac{1}{f_1 + f_2}\left(f_1 I_{1,i}^k + f_2 q_{12}^2 I_{1,i}^k + f_1\eta_{1,i}^k + f_2\eta_{2,i}^k\right)\right) \\
= &\left(\frac{q_{12}^2 f_2 - f_1}{f_1 - f_2} - \frac{q_{12}^2 f_2 + f_1}{f_1 + f_2}\right) I_{1,i}^k \\
&+ \frac{f_1\left(\lambda_1 N_{1,i}^k + \beta_1^k + \epsilon_{1,i}^k\right) - f_2\left(\lambda_2 N_{2,i}^k + \beta_2^k + \epsilon_{2,i}^k\right)}{f_1 - f_2} \\
&- \frac{f_1\eta_{1,i}^k + f_2\eta_{2,i}^k}{f_1 + f_2}.
\end{aligned} \tag{3.27}$$

The scaling of $I_{1,i}^k$ can be easily derived, i.e.

$$\begin{aligned}
\frac{q_{12}^2 f_2 - f_1}{f_1 - f_2} - \frac{q_{12}^2 f_2 + f_1}{f_1 + f_2} &= \frac{\frac{f_1^2}{f_2} - f_1}{f_1 - f_2} - \frac{\frac{f_1^2}{f_2} + f_1}{f_1 + f_2} \\
&= \frac{f_1\left((f_1 - f_2)(f_1 + f_2) - (f_1 + f_2)(f_1 - f_2)\right)}{f_2(f_1 - f_2)(f_1 + f_2)}. \\
&= 0
\end{aligned} \tag{3.28}$$

Eq. (3.27) can be further simplified to

$$\begin{aligned} W_i^k =& \frac{f_1\left(\lambda_1 N_{1,i}^k + \beta_1^k + \epsilon_{1,i}^k\right) - f_2\left(\lambda_2 N_{2,i}^k + \beta_2^k + \epsilon_{2,i}^k\right)}{f_1 - f_2} \\ & - \frac{f_1\eta_{1,i}^k + f_2\eta_{2,i}^k}{f_1 + f_2} \\ =& \lambda_W\left(N_{1,i}^k - N_{2,i}^k + \frac{\beta_1^k}{\lambda_1} - \frac{\beta_2^k}{\lambda_2}\right) + f(\epsilon_{1,i}^k, \epsilon_{2,i}^k, \eta_{1,i}^k, \eta_{2,i}^k), \end{aligned} \tag{3.29}$$

with the widelane wavelength λ_W:

$$\lambda_W = \frac{1}{\frac{1}{\lambda_1} - \frac{1}{\lambda_2}}, \tag{3.30}$$

and the combined noise term

$$f(\epsilon_{1,i}^k, \epsilon_{2,i}^k, \eta_{1,i}^k, \eta_{2,i}^k) = \frac{f_1\epsilon_{1,i}^k - f_2\epsilon_{2,i}^k}{f_1 - f_2} - \frac{f_1\eta_{1,i}^k + f_2\eta_{2,i}^k}{f_1 + f_2}. \tag{3.31}$$

In case of GPS, the wavelength of the widelane Melbourne-Wübbena combination is 86.2 cm, which allows a much easier fixing of ambiguities. In order to eliminate the biases, the double difference Melbourne-Wübbena ΔW_{ij}^{kl} is used:

$$\begin{aligned} \Delta W_{ij}^{kl} &= \left(W_i^k - W_i^l\right) - \left(W_j^k - W_j^l\right) \\ &= \lambda_W\left(\Delta N_{W,ij}^{kl} + \frac{\Delta\beta_{1,ij}^{kl}}{\lambda_1} - \frac{\Delta\beta_{2,ij}^{kl}}{\lambda_2}\right) + f(\Delta\epsilon_{1,ij}^{kl}, \Delta\epsilon_{2,ij}^{kl}, \Delta\eta_{1,ij}^{kl}, \Delta\eta_{2,ij}^{kl}), \end{aligned} \tag{3.32}$$

with

$$\Delta N_{W,ij}^{kl} = \Delta N_{1,ij}^{kl} - \Delta N_{2,ij}^{kl} \tag{3.33}$$

$$\Delta N_{1,ij}^{kl} = (N_{1,i}^k - N_{1,i}^l) - (N_{1,j}^k - N_{1,j}^l) \tag{3.34}$$

$$\Delta N_{2,ij}^{kl} = (N_{2,i}^k - N_{2,i}^l) - (N_{2,j}^k - N_{2,j}^l) \tag{3.35}$$

$$\Delta\beta_{1,ij}^{kl} = (\beta_1^k - \beta_1^l) - (\beta_1^k - \beta_1^l) = 0 \tag{3.36}$$

$$\Delta\beta_{2,ij}^{kl} = (\beta_2^k - \beta_2^l) - (\beta_2^k - \beta_2^l) = 0 \tag{3.37}$$

$$\begin{aligned} f(\Delta\epsilon_{1,ij}^{kl}, \Delta\epsilon_{2,ij}^{kl}, \Delta\eta_{1,ij}^{kl}, \Delta\eta_{2,ij}^{kl}) &= \left(f(\epsilon_{1,i}^k, \epsilon_{2,i}^k, \eta_{1,i}^k, \eta_{2,i}^k - f(\epsilon_{1,i}^l, \epsilon_{2,i}^l, \eta_{1,i}^l, \eta_{2,i}^l)\right) \\ - \left(f(\epsilon_{1,j}^k, \epsilon_{2,j}^k, \eta_{1,j}^k, \eta_{2,j}^k - f(\epsilon_{1,j}^l, \epsilon_{2,j}^l, \eta_{1,j}^l, \eta_{2,j}^l)\right). \end{aligned} \tag{3.38}$$

Combining (3.32) with (3.34) and (3.35) leads to the estimate of the double differenced widelane ambiguity being averaged over time, i.e.

$$\Delta\hat{N}_{W,ij}^{kl} = \left[\frac{1}{T}\sum_{t_n=1}^{T}\frac{\Delta W_{ij}^{kl}(t_n)}{\lambda_W}\right] \tag{3.39}$$

$$\hat{N}_{2,i}^k = \hat{N}_{1,i}^k - \hat{N}_{1,i}^l + \hat{N}_{2,i}^l - \hat{N}_{1,j}^k + \hat{N}_{2,j}^k - \hat{N}_{1,j}^l - \hat{N}_{2,j}^l - \Delta\hat{N}_{W,ij}^{kl}, \tag{3.40}$$

which expresses the ambiguity as a linear combination of 7 others and a measurement combination.

Example

The first two equations of Eq. (3.1) can be expressed as a matrix expression, i.e.

$$\begin{aligned}\begin{pmatrix} \lambda_1\phi_1 \\ \lambda_2\phi_2 \end{pmatrix} &= \begin{pmatrix} \lambda_1\mathbb{1} & 0 \\ 0 & \lambda_2\mathbb{1} \end{pmatrix} \begin{pmatrix} N_1 \\ N_2 \end{pmatrix} + f\left(g, I_1, \beta_{1,R}, \beta_1^K, \epsilon_1\right) \\ &= H_N \begin{pmatrix} N_1 \\ N_2 \end{pmatrix} + f\left(g, I_1, \beta_{1,R}, \beta_1^K, \epsilon_1\right). \end{aligned} \tag{3.41}$$

The a priori knowledge of widelane ambiguities results in additional measurements or - in an alternative interpretation - enables a reduction of unknowns.

A set of 2 stations each seeing the same 3 satellites can be described as

$$H_N \begin{pmatrix} N_1 \\ N_2 \end{pmatrix} = \begin{pmatrix} \lambda_1 & 0 & 0 & 0 & 0 & 0 & 0 & 0 & 0 & 0 & 0 & 0 \\ 0 & \lambda_1 & 0 & 0 & 0 & 0 & 0 & 0 & 0 & 0 & 0 & 0 \\ 0 & 0 & \lambda_1 & 0 & 0 & 0 & 0 & 0 & 0 & 0 & 0 & 0 \\ 0 & 0 & 0 & \lambda_1 & 0 & 0 & 0 & 0 & 0 & 0 & 0 & 0 \\ 0 & 0 & 0 & 0 & \lambda_1 & 0 & 0 & 0 & 0 & 0 & 0 & 0 \\ 0 & 0 & 0 & 0 & 0 & \lambda_1 & 0 & 0 & 0 & 0 & 0 & 0 \\ 0 & 0 & 0 & 0 & 0 & 0 & \lambda_2 & 0 & 0 & 0 & 0 & 0 \\ 0 & 0 & 0 & 0 & 0 & 0 & 0 & \lambda_2 & 0 & 0 & 0 & 0 \\ 0 & 0 & 0 & 0 & 0 & 0 & 0 & 0 & \lambda_2 & 0 & 0 & 0 \\ 0 & 0 & 0 & 0 & 0 & 0 & 0 & 0 & 0 & \lambda_2 & 0 & 0 \\ -\lambda_2 & -\lambda_2 & 0 & -\lambda_2 & \lambda_2 & 0 & -\lambda_2 & \lambda_2 & 0 & \lambda_2 & 0 & 0 \\ 0 & 0 & 0 & 0 & 0 & 0 & 0 & 0 & 0 & 0 & 0 & \lambda_2 \end{pmatrix} \begin{pmatrix} N_{1,1}^1 \\ N_{1,1}^2 \\ N_{1,1}^3 \\ N_{1,2}^1 \\ N_{1,2}^2 \\ N_{1,2}^3 \\ N_{2,1}^1 \\ N_{2,1}^2 \\ N_{2,1}^3 \\ N_{2,2}^1 \\ N_{2,2}^2 \\ N_{2,2}^3 \end{pmatrix} + cor, \tag{3.42}$$

with

$$cor = \begin{pmatrix} 0 \\ 0 \\ 0 \\ 0 \\ 0 \\ 0 \\ 0 \\ 0 \\ 0 \\ 0 \\ -\Delta\hat{N}_{W,2,1}^{2,1} \\ 0 \end{pmatrix}. \tag{3.43}$$

The red column in (3.42) corresponding to the red mapped ambiguity can be removed after mapping, which consists in filling the corresponding row with the adequate terms and adding a correction vector *cor* which contains the last term of equation (3.39). If a common reference station is chosen for all Melbourne-Wübbena combinations and all stations have the same visibility, the number

of ambiguities being mapped is $K(R-1)$. This a priori knowledge allows to reduce the number of unknown ambiguities and therefore contributes to a faster estimation of phase biases.

3.4 Melbourne-Wübbena Combination for Undifferenced Measurements

The elimination of both geometry and ionospheric delays by the Melbourne-Wübbena combination results in an extremely stable behaviour over time also for undifferenced measurements. Fig. 3.1 shows the fractional widelane bias for an CORS station over one month.

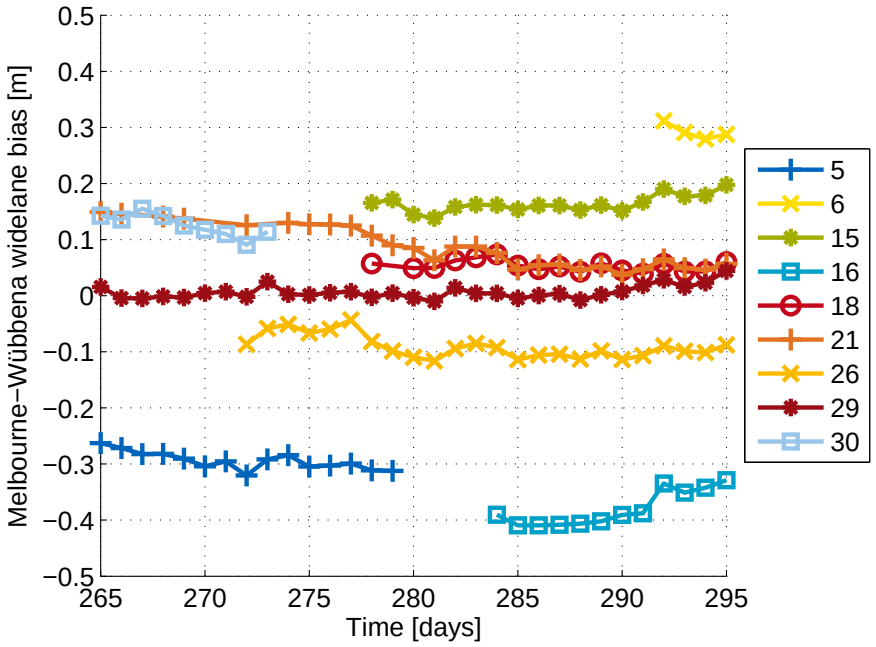

Figure 3.1: Stability of Melbourne-Wübbena combination bias: This linear combination is applied to 1 Hz measurements (22.09.-22.10.2011) from CORS station MTUM, and averaged over the first two hours of each day. One can observe a high stability over a whole month, which enables a transmission as correction parameter for widelane ambiguity fixing and, thus, an ambiguity fixing at the receiver.

Chapter 4

Cascaded Kalman Filter

In the previous chapter, the system of equations (3.1) was transformed by a set of parameter mappings into Eq. (3.25), which then becomes solvable. A first Kalman filter [12] is introduced to estimate the geometry, ionospheric slant delays, integer ambiguities and phase biases, using code and phase measurements on both frequencies. The integer ambiguities are resolved sequentially based on the convergence behavior over a period of time. The geometry estimates are split into terms of orbital errors, receiver clock offsets and satellite code biases, etc., which are to be estimated in a second-stage Kalman filter. However, the assumption of a traditional Kalman filter is that measurement noises are not correlated over time. It can be shown that the geometry estimates are yet correlated in this sense. The Bryson method is used to decouple the measurement noise in the second Kalman filter. In the last section, a cascaded Kalman filter is set up with the Bryson method applied to the second stage. Simulation results show that the error in orbital error estimates is smaller than 2 cm.

4.1 Standard Kalman Filter

The measurement and state space models of a conventional Kalman filter [12] are given by

$$\begin{aligned} &x_n = \Phi_{n-1} x_{n-1} + w_{n-1} \\ &z_n = H_n x_n + \zeta_n \\ &E(w_n) = E(\zeta_n) = 0 \\ &E(w_k w_l^{\mathrm{T}}) = Q_k \delta_{kl}, \quad E(\zeta_k \zeta_l^{\mathrm{T}}) = R_k \delta_{kl}, \quad E(w_k \zeta_l^{\mathrm{T}}) = 0, \end{aligned} \tag{4.1}$$

with δ_{kl} being the Kronecker delta function

$$\delta_{kl} = \begin{cases} 1, & \text{if } k = l \\ 0, & \text{if } k \neq l \end{cases}.$$

The state vector x_n contains the geometry terms, ionospheric slant delays, integer ambiguities and phase biases given by E.(3.25), i.e.

$$x_n = \left(\tilde{g}_n^{\mathrm{T}}, \dot{\tilde{g}}_n^{\mathrm{T}}, \ddot{\tilde{g}}_n^{\mathrm{T}}, \tilde{I}_n^{\mathrm{T}}, \tilde{\tilde{\beta}}_R^{\mathrm{T}}, \tilde{\tilde{\beta}}^{K,\mathrm{T}}, \tilde{N}^{\mathrm{T}} \right)^{\mathrm{T}}. \tag{4.2}$$

The measurement vector z_n contains the absolute code and phase measurements on two frequencies, i.e.

$$z_n = \left(\lambda_1 \varphi_{1,n}^{\mathrm{T}}, \lambda_2 \varphi_{2,n}^{\mathrm{T}}, \rho_{1,n}^{\mathrm{T}}, \rho_{2,n}^{\mathrm{T}}\right)^{\mathrm{T}}. \tag{4.3}$$

The process and measurement noises w_n and ζ_n are assumed to be white, of zero mean and with Q_n and R_n as their respective covariance matrices.

In the following, it is assumed that a number of K_i satellites is visible to receiver i ($i \in [1, R]$). The number of measurements N_{MEAS} on a single frequency for the code (or the phase) is given by

$$N_{\mathrm{MEAS}} = \sum_{i=1}^{R} K_i. \tag{4.4}$$

Using Eq.(3.4), the state transition matrix Φ_n can be obtained by

$$\Phi_n = \begin{pmatrix} \mathbb{1} & \Delta t \mathbb{1} & \frac{1}{2}\Delta t^2 \mathbb{1} & 0 & 0 & 0 & 0 \\ 0 & \mathbb{1} & \Delta t \mathbb{1} & 0 & 0 & 0 & 0 \\ 0 & 0 & \mathbb{1} & 0 & 0 & 0 & 0 \\ 0 & 0 & 0 & \mathbb{1} & 0 & 0 & 0 \\ 0 & 0 & 0 & 0 & \mathbb{1} & 0 & 0 \\ 0 & 0 & 0 & 0 & 0 & \mathbb{1} & 0 \\ 0 & 0 & 0 & 0 & 0 & 0 & \mathbb{1} \end{pmatrix}, \tag{4.5}$$

with $\mathbb{1}$ representing the identity matrix having different dimensions depending on each state.

The H_n matrix represents the relationships between states and measurements at the discrete time instant t_n. It can be separated into sub-matrices, i.e.

$$H_n = \begin{pmatrix} H_{\tilde{g}} & H_{\dot{\tilde{g}}} & H_{\ddot{\tilde{g}}} & H_{\tilde{I}} & H_{\underset{\tilde{\beta}_R}{\tilde{z}}} & H_{\underset{\beta^K}{\tilde{z}}} & H_{\tilde{N}} \end{pmatrix}. \tag{4.6}$$

The $H_{\tilde{g}}$, $H_{\dot{\tilde{g}}}$ and $H_{\ddot{\tilde{g}}}$ are straightforward to be obtained since the geometry term appears in every equations of the base model:

$$H_{\tilde{g}} = \mathbb{1}^{4N_{\mathrm{MEAS}} \times N_{\mathrm{MEAS}}} \tag{4.7}$$

$$H_{\dot{\tilde{g}}} = H_{\ddot{\tilde{g}}} = 0. \tag{4.8}$$

Since the code and phase measurements have opposite signs on ionosphere, the $H_{\tilde{I}}$ matrix is given by

$$H_{\tilde{I}} = \begin{pmatrix} -1 \\ -q_{12}^2 \\ 1 \\ q_{12}^2 \end{pmatrix} \otimes \mathbb{1}^{N_{\mathrm{MEAS}} \times N_{\mathrm{MEAS}}}, \tag{4.9}$$

with $\otimes$ being the Kronecker product.

$H_{\underset{\tilde{\beta}_R}{\tilde{z}}}$ has a specific form depending on how the measurements are sorted. The following order is taken

$$z_n = \left(\lambda_1 \varphi_{1,n}^{\mathrm{T}}, \lambda_2 \varphi_{2,n}^{\mathrm{T}}, \rho_{1,n}^{\mathrm{T}}, \rho_{2,n}^{\mathrm{T}}\right)^{\mathrm{T}}. \tag{4.10}$$

with

$$\varphi_{m,n} = \left(\varphi^1_{m,1,n} \cdots \lambda_1 \varphi^1_{m,R,n} \cdots \lambda_1 \varphi^{K_R}_{m,R,n}\right)^{\mathrm{T}}$$
$$\rho_{m,n} = \left(\rho^1_{m,1,n} \cdots \rho^1_{m,R,n} \cdots \rho^{K_R}_{m,R,n}\right)^{\mathrm{T}} \tag{4.11}$$

Accordingly, $H_{\underset{\beta_R}{\tilde{z}}}$ is described by

$$H_{\underset{\beta_R}{\tilde{z}}} = \begin{pmatrix} \mathbb{1}^{2\times 2} \\ 0^{2\times 2} \end{pmatrix} \otimes \begin{pmatrix} \mathbb{1}^{K_1\times 1} & & & \\ & \mathbb{1}^{K_2\times 1} & & \\ & & \ddots & \\ & & & \mathbb{1}^{K_R\times 1} \end{pmatrix}. \tag{4.12}$$

The $H_{\underset{\beta^K}{\tilde{z}}}$ is a $4N_{\mathrm{MEAS}} \times 2(K-1)$ matrix (see (3.18)). The $H_{\tilde{N}}$ depends on Gaussian elimination operation but is based on the original H_N matrix, which is given by

$$H_N = \begin{pmatrix} \lambda_1 & 0 \\ 0 & \lambda_2 \\ 0 & 0 \\ 0 & 0 \end{pmatrix} \otimes \mathbb{1}^{N_{\mathrm{MEAS}}}. \tag{4.13}$$

The Kalman filter is a recursive least-squares estimator, which benefits from the joint use of a measurement and state space model, and is in general implemented in two steps:

$$\text{Prediction step} \qquad \begin{aligned} \hat{x}_n^- &= \Phi_{n-1}\hat{x}_{n-1}^+ \\ P_n^- &= \Phi_{n-1}P_{n-1}^+\Phi_{n-1}^{\mathrm{T}} + Q_{n-1} \end{aligned} \tag{4.14}$$

$$\text{Update step} \qquad \begin{aligned} K_n &= P_n^- H_n^{\mathrm{T}} \left(H_n P_n^- H_n^{\mathrm{T}} + R_n\right)^{-1} \\ \hat{x}_n^+ &= \hat{x}_n^- + K_n\left(z_n - H_n\hat{x}_n^-\right) \\ P_n^+ &= \left(I - K_n H_n\right) P_n^-, \end{aligned} \tag{4.15}$$

where

Q_n	:	covariance of the process noise
R_n	:	covariance of the measurement error
K_n	:	Kalman gain
P_n^-	:	a priori error covariance matrix
P_n^+	:	a posteriori error covariance matrix.

In the prediction step, an a priori estimate of the state $\hat{x}_n^-$ is computed from the posteriori estimate of the previous epoch or an initial value. The update step serves as a refinement by using the measurements of the current time instant and builds an a posteriori state estimate $\hat{x}_n^+$.

The initialization of the Kalman filter is done with a least-squares estimation using the measurements of the first 3 epochs (3 time instants are needed to

produce a reliable second derivative estimate of the geometry term), i.e.

$$\begin{pmatrix} z_1 \\ z_2 \\ z_3 \end{pmatrix} = H_0 \cdot \begin{pmatrix} x_1 \\ x_2 \\ x_3 \end{pmatrix} + \begin{pmatrix} v_1 \\ v_2 \\ v_3 \end{pmatrix}, \tag{4.16}$$

with x_1, x_2, x_3 being the first 3 state vectors without $\dot{\tilde{g}}$ and $\ddot{\tilde{g}}$ in Eq.(4.2) and with

$$H_0 = \begin{pmatrix} \mathbb{1}^{3\times 3} \otimes H_{\tilde{g}} & \mathbb{1}^{3\times 1} \otimes (H_{\tilde{I}} & H_{\substack{\tilde{\xi} \\ \tilde{\beta}_R}} & H_{\substack{\tilde{\xi} \\ \tilde{\beta}^K}} & H_{\tilde{N}}) \end{pmatrix}. \tag{4.17}$$

The initial state vector is calculated by performing the least-squares estimation

$$\begin{pmatrix} \hat{x}_1 \\ \hat{x}_2 \\ \hat{x}_3 \end{pmatrix} = \left(H_0^{\mathrm{T}} \Sigma_0^{-1} H_0\right)^{-1} H_0^{\mathrm{T}} \Sigma_0^{-1} \cdot \begin{pmatrix} z_1 \\ z_2 \\ z_3 \end{pmatrix}, \tag{4.18}$$

with

$$\Sigma_0 = \mathbb{1}^{3\times 3} \otimes R_0. \tag{4.19}$$

Then, the initial state estimates of the geometry term derivatives are computed by differencing between the estimated geometry terms on three time instants.

During the Kalman filtering, an ambiguity resolution is performed to improve the accuracy of all other states [11]. Without ambiguity resolution, the ambiguities estimates would stay as float numbers whereas ambiguities are integers by definition. Once an ambiguity has been fixed to the right integer value, it is removed from the state vector allowing a more precise estimate of the phase biases. The fixing criterion is based on 3 parameters: a fixing window of length t_{fixing} epochs, a threshold ϵ_{fixing} and a probability α_{fixing} (allowing some outliers) expressed in percentage. At each epoch t_n, the integer $N^k_{int,i}$ closest to $\hat{N}^k_i(t_n)$ is computed as well as its distance from each previous $\hat{N}^k_i$ during the time period t_{fixing} [9]. One ambiguity is only fixed when the offsets between float and integer numbers are below a certain threshold over a time window, i.e.

$$\#\left\{\hat{N}^k_i(t), \left|\hat{N}^k_i(t) - N^k_{int,i}\right| < \epsilon_{\text{fixing}}; t \in \{t_n - t_{\text{fixing}}, \ldots, t_n\}\right\} < \alpha_{\text{fixing}} \cdot t_{\text{fixing}}, \tag{4.20}$$

with # denoting the cardinality of a set. In this work, the parameters are chosen to be

$$t_{\text{fixing}} = 100 \text{ epochs}, \quad \epsilon_{\text{fixing}} = 0.05\text{cycles}, \quad \alpha_{\text{fixing}} = 95\ \%.$$

4.2 The Bryson Model

In order to take the correlation between the measurements over time in the second Kalman filter into account, Bryson and Henrikson [13] proposed a method to decouple the measurements, i.e.

$$x_n = \Phi_{n-1} x_{n-1} + w_{n-1} \tag{4.21}$$

$$z_n = H_n x_n + v_n \tag{4.22}$$

$$v_n = \Gamma_{n-1} v_{n-1} + \zeta_n, \tag{4.23}$$

where v_n denotes the measurement noise in the second Kalman filter, Γ_n describes the temporal correlation introduced by an earlier filtering process, and ζ_n is white Gaussian distributed noise. Obviously, the main difference between this model and the one underlying conventional Kalman filters lies in the description of the measurement noise, which is white Gaussian for the standard one and colored for this much more general model. Clearly, Bryson's model includes the conventional model as a special case.

The statistic properties of the process and measurement noises are given by

$$E(w_n) = E(\zeta_n) = 0 \tag{4.24}$$

$$E(w_n w_m^{\mathrm{T}}) = Q_n \delta_{nm} \tag{4.25}$$

$$E(\zeta_n \zeta_m^{\mathrm{T}}) = R_n \delta_{nm} \tag{4.26}$$

$$E(w_n \zeta_m^{\mathrm{T}}) = 0. \tag{4.27}$$

By time-differencing the measurements, according to (4.21), (4.22) a new measurement z_n^* can be derived as

$$\begin{aligned} z_n^* &= z_{n+1} - \Gamma_n z_n \\ &= H_{n+1} x_{n+1} + v_{n+1} - \Gamma_n \left(H_n x_n + v_n \right) \\ &= H_{n+1} \left(\Phi_n x_n + w_n \right) + \Gamma_n v_n + \zeta_{n+1} - \Gamma_n H_n x_n - \Gamma_n v_n \\ &= \left(H_{n+1} \Phi_n - \Gamma_n H_n \right) x_n + H_{n+1} w_n + \zeta_{n+1} \\ &= H_n^* x_n + v_n^*, \end{aligned} \tag{4.28}$$

with

$$H_n^* = H_{n+1} \Phi_n - \Gamma_n H_n \tag{4.29}$$

$$v_n^* = H_{n+1} w_n + \zeta_{n+1}. \tag{4.30}$$

where v_n^* represents the new measurement error with zero mean and covariance matrix R_n^*, and is no longer correlated over time, i.e.

$$E\{v_n^*\} = 0, \tag{4.31}$$

$$\begin{aligned} E\{v_n^* v_m^{*\mathrm{T}}\} &= E\{ \left(H_{n+1} w_n + \zeta_{n+1} \right) \left(H_{m+1} w_m + \zeta_{m+1} \right) \} \\ &= \left(H_{n+1} Q_n H_{n+1}^{\mathrm{T}} + R_{n+1} \right) \delta_{nm} \\ &= R_n^* \delta_{nm}. \end{aligned} \tag{4.32}$$

However, a correlation between the process noise w_n and the new measurement noise v_n^* is introduced as

$$\begin{aligned} E\{w_n v_m^{*\mathrm{T}}\} &= E\{ w_n \left(H_{m+1} w_m + \zeta_{m+1} \right)^{\mathrm{T}} \} \\ &= \left(Q_n H_{n+1}^{\mathrm{T}} \right) \delta_{nm} \\ &= S_n \delta_{nm}. \end{aligned} \tag{4.33}$$

Thus, a new state process noise vector w_n^* shall be introduced accordingly which is following a white Gaussian noise distribution with covariance Q_n^* and has no correlation with the measurement noise v_n^*, i.e.

$$E\{w_n^*\} = 0 \tag{4.34}$$

$$E\{w_n^* w_m^{*\mathrm{T}}\} = Q_n^* \delta_{nm} \tag{4.35}$$

$$E\{w_n^* v_m^{*\mathrm{T}}\} = 0. \tag{4.36}$$

The state transition in Eq.(4.21) remains unchanged after adding a 0, which is obtained according to (4.28) by

$$z_{n-1}^* - H_{n-1}^* x_{n-1} - v_{n-1}^* = 0. \tag{4.37}$$

A new matrix J_n is introduced into the state transition by

$$\begin{aligned} x_n &= \Phi_{n-1} x_{n-1} + w_{n-1} + J_{n-1}\left(z_{n-1}^* - H_{n-1}^* x_{n-1} - v_{n-1}^*\right) \\ &= \left(\Phi_{n-1} - J_{n-1} H_{n-1}^*\right) x_{n-1} + J_{n-1} z_{n-1}^* + \left(w_{n-1} - J_{n-1} v_{n-1}^*\right) \\ &= \Phi_{n-1}^* x_{n-1} + J_{n-1} z_{n-1}^* + w_{n-1}^*, \end{aligned} \tag{4.38}$$

with

$$\Phi_n^* = \Phi_n - J_n H_n^* \tag{4.39}$$

$$w_n^* = w_n - J_n v_n^*. \tag{4.40}$$

According to (4.36) and (4.40), the cross correlation between process noise and measurement noise is obtained by

$$\begin{aligned} E\{w_n^* v_m^{*\mathrm{T}}\} &= E\{(w_n - J_n v_n^*)\, v_m^{*\mathrm{T}}\} \\ &= S_n \delta_{nm} - J_n R_n^* \delta_{nm} \qquad (4.41) \\ &= 0. \qquad (4.42) \end{aligned}$$

The expression of J_n is given by

$$J_n = S_n \left(R_n^*\right)^{-1}, \tag{4.43}$$

and Q_n^* can be derived as

$$\begin{aligned} Q_n^* &= E\{w_n^* w_n^{*\mathrm{T}}\} \\ &= E\{(w_n - J_n v_n^*)(w_n - J_n v_n^*)^{\mathrm{T}}\} \\ &= E\{w_n w_n^{\mathrm{T}}\} - E\{w_n v_n^{*\mathrm{T}}\} J_n^{\mathrm{T}} - J_n E\{v_n^* w_n^{\mathrm{T}}\} + J_n E\{v_n^* v_n^{*\mathrm{T}}\} J_n^{\mathrm{T}} \\ &= Q_n - S_n J_n^{\mathrm{T}} - J_n S_n^{\mathrm{T}} + J_n R_n^* J_n^{\mathrm{T}} \\ &= Q_n - S_n J_n^{\mathrm{T}} - S_n \left(R_n^*\right)^{-1} S_n^{\mathrm{T}} + S_n \left(R_n^*\right)^{-1} Rn^* J_n^{\mathrm{T}} \\ &= Q_n - S_n \left(R_n^*\right)^{-1} S_n^{\mathrm{T}}. \end{aligned} \tag{4.44}$$

The final set of the new introduced variables is obtained as

$$\begin{aligned} z_n^* &= z_{n+1} - \Gamma_n z_n \\ H_n^* &= H_{n+1}\Phi_n - \Gamma_n H_n \\ S_n &= Q_n H_{n+1}^{\mathrm{T}} \\ R_n^* &= H_{n+1} Q_n H_{n+1}^{\mathrm{T}} + R_{n+1} \\ J_n &= S_n \left(R_n^*\right)^{-1} \\ Q_n^* &= Q_n - S_n \left(R_n^*\right)^{-1} S_n^{\mathrm{T}} \\ \Phi_n^* &= \Phi_n - J_n H_n^*. \end{aligned} \tag{4.45}$$

The new prediction and updating steps are stated as

$$\text{Prediction} \qquad \begin{aligned} \hat{x}_n^- &= \Phi_{n-1}^* \hat{x}_{n-1}^+ + J_{n-1} z_{n-1}^* \\ P_n^- &= \Phi_{n-1}^* P_{n-1}^+ \Phi_{n-1}^{*\mathrm{T}} + Q_{n-1}^* \end{aligned} \tag{4.46}$$

$$
\begin{aligned}
& & K_n &= P_n^- H_n^{*\mathrm{T}} \left(H_n^* P_n^- H_n^{*\mathrm{T}} + R_n^* \right)^{-1} \\
\text{Updating} & & \hat{x}_n^+ &= \hat{x}_n^- + K_n \left(z_n^* - H_n^* \hat{x}_n^- \right) \\
& & P_n^+ &= \left(I - K_n H_n^* \right) P_n^-
\end{aligned}
\tag{4.47}
$$

The algorithm is very similar to the equations (4.14) and (4.15) with the usage of the 'newly' time uncorrelated defined variables z_n^*, H_n^*, R_n^*, Q_n^* and Φ_n^*.

4.3 Cascaded Kalman Filter

A cascaded Kalman filter has the advantage that it enables a *faster ambiguity resolution* compared to an estimation of all unknowns in one single step. However, the cascading of filters introduces time correlation into the a posteriori estimates, such that the assumption of white Gaussian measurement noise is no longer fulfilled for all filters except the first one. Therefore, the method of Bryson shall be used to decouple the filters. Cascading Kalman filters is also advantageous as batch processing of a large number of states is computationally challenging.

4.3.1 First Stage

The first Kalman filter focuses on an accurate estimation of the geometry term $\Delta\tilde{g}_i^k$. The measurement model of Eq. (3.25) shall be slightly modified, i.e. an a priori knowledge of the receiver and satellite positions (and, thus, the range) as well as of the tropospheric delay shall be assumed available and, thus, only the errors of this model have to be estimated, i.e.

$$
\begin{aligned}
\lambda_1 \Delta\phi_{1,i}^k(t_n) &= \Delta\tilde{g}_i^k(t_n) - \tilde{I}_{1,i}^k(t_n) + \lambda_1 \tilde{N}_{1,i}^k + \tilde{\tilde{\beta}}_{1,i} + \tilde{\tilde{\beta}}_1^k + \epsilon_{1,i}^k(t_n) \\
\lambda_2 \Delta\phi_{2,i}^k(t_n) &= \Delta\tilde{g}_i^k(t_n) - q_{12}^2 \tilde{I}_{1,i}^k(t_n) + \lambda_2 \tilde{N}_{2,i}^k + \tilde{\tilde{\beta}}_{2,i} + \tilde{\tilde{\beta}}_2^k + \epsilon_{2,i}^k(t_n), \\
\Delta\rho_{1,i}^k(t_n) &= \Delta\tilde{g}_i^k(t_n) + \tilde{I}_{1,i}^k(t_n) + \eta_{1,i}^k(t_n) \\
\Delta\rho_{2,i}^k(t_n) &= \Delta\tilde{g}_i^k(t_n) + q_{12}^2 \tilde{I}_{1,i}^k(t_n) + \eta_{2,i}^k(t_n)
\end{aligned}
\tag{4.48}
$$

where the geometry term is written as

$$
\Delta\tilde{g}_i^k(t_n) = \vec{e}_i^{k\mathrm{T}} \Delta\vec{r}^k(t_n) + c\delta\tau_i + b_{g^k}, \tag{4.49}
$$

with $c\delta\tau_i$ being the receiver clock offset, b_{g^k} being the satellite code bias and with $\Delta\vec{r}^K$ defining the orbital error of the satellite, i.e.

$$
\Delta\vec{r}^k = \vec{r}^k - \hat{\vec{r}}^k. \tag{4.50}
$$

Both the geometry term and the slant ionospheric delay of the first Kalman filter include a deterministic first order dynamical model and a Gauss-Markov process, i.e.

$$
\Delta\tilde{g}_i^k(t_n) = \Delta\tilde{g}_i^k(t_{n-1}) + \Delta t \Delta\dot{\tilde{g}}_i^k(t_{n-1}) + w_{\Delta\tilde{g}_i^k}(t_n) \tag{4.51}
$$

$$
\tilde{I}_{m,i}^k(t_n) = \tilde{I}_{m,i}^k(t_{n-1}) + \Delta t \dot{\tilde{I}}_{m,i}(t_{n-1}) + w_{\tilde{I}_i^k}(t_n). \tag{4.52}
$$

The state vector for the first Kalman filter is obtained as

$$x_n^{(1)} = \left[\Delta\tilde{g}_n^{\mathrm{T}}, \Delta\dot{\tilde{g}}_n^{\mathrm{T}}, \tilde{I}_n^{\mathrm{T}}, \dot{\tilde{I}}_n^{\mathrm{T}}, \tilde{\tilde{\beta}}_R^{\mathrm{T}}, \tilde{\tilde{\beta}}^{K,\mathrm{T}}, \tilde{N}^{\mathrm{T}}\right]^{\mathrm{T}}, \tag{4.53}$$

where the upper index $^{(1)}$ indicates the stage of Kalman filters.

The measurement vector combines 2 epochs together to allow a better estimate of the first derivatives,

$$z_n^{(1)} = \left[\lambda_1\varphi_{1,n}^{\mathrm{T}}, \lambda_2\varphi_{2,n}^{\mathrm{T}}, \rho_{1,n}^{\mathrm{T}}, \rho_{2,n}^{\mathrm{T}}, \lambda_1\varphi_{1,n+1}^{\mathrm{T}}, \lambda_2\varphi_{2,n+1}^{\mathrm{T}}, \rho_{1,n+1}^{\mathrm{T}}, \rho_{2,n+1}^{\mathrm{T}}\right]^{\mathrm{T}}. \tag{4.54}$$

The new number of states is calculated as

$$\begin{aligned} N_{\mathrm{STATES}} &= N_{\mathrm{meas}} + N_{\mathrm{meas}} + N_{\mathrm{meas}} + N_{\mathrm{meas}} + 2R + 2(K-1) \\ &\quad + 2N_{\mathrm{meas}} - 2R - 2(K-1) \\ &= 6N_{\mathrm{meas}}, \end{aligned} \tag{4.55}$$

with K being the number of visible satellites, and R is the number of stations. It is noted that in the above calculation, the Gaussian elimination has already been applied to the ambiguities and, thus, no singularity is expected with the phase biases.

The state transition matrix can be derived from (4.51) and (4.52) as

$$\Phi_n = \begin{pmatrix} \mathbb{1} & \Delta t\mathbb{1} & 0 & 0 & 0 & 0 & 0 \\ 0 & \mathbb{1} & 0 & 0 & 0 & 0 & 0 \\ 0 & 0 & \mathbb{1} & \Delta t\mathbb{1} & 0 & 0 & 0 \\ 0 & 0 & 0 & \mathbb{1} & 0 & 0 & 0 \\ 0 & 0 & 0 & 0 & \mathbb{1} & 0 & 0 \\ 0 & 0 & 0 & 0 & 0 & \mathbb{1} & 0 \\ 0 & 0 & 0 & 0 & 0 & 0 & \mathbb{1} \end{pmatrix}, \tag{4.56}$$

with $\Delta t = 2$ epochs in this model because of the form of the measurements.

According to the system model the H_n matrix has the following form:

$$H_n = \begin{pmatrix} H_{\Delta\tilde{g}} & 0 & H_{\tilde{I}} & 0 & H_{\tilde{\tilde{\beta}}_R} & H_{\tilde{\tilde{\beta}}^K} & H_{\tilde{N}} \\ H_{\Delta\tilde{g}} & \Delta t H_{\Delta\tilde{g}} & H_{\tilde{I}} & \Delta t H_{\tilde{I}} & H_{\tilde{\tilde{\beta}}_R} & H_{\tilde{\tilde{\beta}}^K} & H_{\tilde{N}} \end{pmatrix}, \tag{4.57}$$

where $H_{\Delta\tilde{g}}$, H_{β_R}, H_{β^K}, H_I and $H_{\tilde{N}}$ matrices are defined like in the previous model.

In this work, the standard deviation of the measurement noises are chosen according to [14][15], i.e.

$$\begin{aligned} \sigma_\phi &= 5 \text{ mm} &&: \text{ phase noise} \\ \sigma_{\rho_{E1}} &= 11.14 \text{ cm} &&: \text{ E1 code noise} \\ \sigma_{\rho_{E5}} &= 1.93 \text{ cm} &&: \text{ E5 code noise.} \end{aligned}$$

Since the geometry term $\Delta\tilde{g}$ consists of different parameters, its process noise matrix $Q_{\Delta\tilde{g}}$ is derived from the process noise matrix of those parameters,

i.e.

$$Q_{\Delta\tilde{g}} = H_{\Delta\vec{r}^K} Q_{\Delta\vec{r}^K} H_{\Delta\vec{r}^K}^{\mathrm{T}} + H_{c\delta\tau_R} Q_{c\delta\tau_R} H_{c\delta\tau_R}^{\mathrm{T}}, \tag{4.58}$$

with $H_{\Delta\vec{r}^K}$, $H_{c\delta\tau_R}$, $Q_{\Delta\vec{r}^K}$ and $Q_{c\delta\tau_R}$ being respectively the state transition matrix and process noise covariance matrix of the satellite position error $\Delta\vec{r}^K$ and the receiver clock offset $c\delta\tau_R$. The satellite code bias b_{g^k} is assumed to be constant over time and thus does not appear in the above equation.

4.3.2 Computation of the Time-Correlation

The main idea is to use the Bryson method with the second stage Kalman filter, while the standard Kalman filter is used for the first stage. The measurements $z_n^{(2)}$ of the second stage are then equal to the a posteriori state estimate $\hat{x}_n^{+(1)}$ of the first stage. To perform the filtering of the second stage, the matrix Γ_n representing the time correlation of the measurement noise has to be computed. It can be performed by calculating the correlation matrix between the a posteriori state estimate of the first Kalman filter at epoch n and $n+1$. To simplify notations all the matrices except Γ_n are referring to the first Kalman filter in this section.

The temporal correlation of the *posteriori state estimates* of the first Kalman filter, which also equals the temporal correlation of the *measurements* of the second Kalman filter, is calculated as

$$\begin{aligned} &E\{\left(\hat{x}_n^{+(1)} - E\{\hat{x}_n^{+(1)}\}\right)\left(\hat{x}_{n+1}^{+(1)} - E\{\hat{x}_{n+1}^{+(1)}\}\right)^{\mathrm{T}}\} \\ &= E\{(z_n^{(2)} - E\{z_n^{(2)}\})(z_{n+1}^{(2)} - E\{z_{n+1}^{(2)}\})^{\mathrm{T}}\} \\ &= E\{v_n^{(2)} v_{n+1}^{(2)\mathrm{T}}\}. \end{aligned} \tag{4.59}$$

According to Eq. (4.23), the temporal correlation of measurement noise of the second Kalman filter is obtained by

$$\begin{aligned} E\{v_n^{(2)} v_{n+1}^{(2)\mathrm{T}}\} &= E\{v_n^{(2)}(\Gamma_n v_n^{(2)} + \zeta_n^{(2)})^{\mathrm{T}}\} \\ &= E\{v_n^{(2)} v_n^{(2)\mathrm{T}}\}\Gamma_n^{\mathrm{T}}, \end{aligned} \tag{4.60}$$

where the noise covariance is defined as

$$\begin{aligned} E\{v_n^{(2)} v_n^{(2)\mathrm{T}}\} &= E\{(z_n^{(2)} - E\{z_n^{(2)}\})(z_n^{(2)} - E\{z_n^{(2)}\})^{\mathrm{T}}\} \\ &= E\{(\hat{x}_n^{+(1)} - x_n^{(1)})(\hat{x}_n^{+(1)} - x_n^{(1)})^{\mathrm{T}}\} \\ &= P_{\hat{x}_n^+}. \end{aligned} \tag{4.61}$$

Since

$$\begin{aligned} \hat{x}_{n+1}^{+(1)} - x_{n+1}^{(1)} &= \hat{x}_{n+1}^{-(1)} + K_{n+1}(z_{n+1}^{(1)} - H_{n+1}\hat{x}_{n+1}^{-(1)}) - x_{n+1}^{(1)} \\ &= (I - K_{n+1}H_{n+1})\hat{x}_{n+1}^{-(1)} + K_{n+1}(H_{n+1}x_{n+1}^{(1)} + \zeta_{n+1}^{(1)}) - x_{n+1}^{(1)} \\ &= (I - K_{n+1}H_{n+1})(\hat{x}_{n+1}^{-(1)} - x_{n+1}^{(1)}) + K_{n+1}\zeta_{n+1}^{(1)}, \end{aligned} \tag{4.62}$$

another way to calculate the cross-correlation of the state estimates is given by

$$\begin{aligned}
&E\{\left(\hat{x}_n^{+(1)} - E\{\hat{x}_n^{+(1)}\}\right)\left(\hat{x}_{n+1}^{+(1)} - E\{\hat{x}_{n+1}^{+(1)}\}\right)^{\mathrm{T}}\} \\
&= E\{\left(\hat{x}_n^{+(1)} - x_n^{(1)}\right)\left(\hat{x}_{n+1}^{+(1)} - x_{n+1}^{(1)}\right)^{\mathrm{T}}\} \\
&= E\{(\hat{x}_n^{+(1)} - x_n^{(1)})(\hat{x}_{n+1}^{-(1)} - x_{n+1}^{(1)})^{\mathrm{T}}\}(I - K_{n+1}H_{n+1})^{\mathrm{T}} \\
&= E\{(\hat{x}_n^{+(1)} - x_n^{(1)})(\Phi_n(\hat{x}_n^{+(1)} - x_n^{(1)}) - w_n^{(1)})^{\mathrm{T}}\}(I - K_{n+1}H_{n+1})^{\mathrm{T}} \\
&= (P_{\hat{x}_n^+}\Phi_n^{\mathrm{T}} - E\{(\hat{x}_n^{+(1)} - x_n^{(1)})w_n^{(1)\mathrm{T}}\})(I - K_{n+1}H_{n+1})^{\mathrm{T}} \\
&= P_{\hat{x}_n^+}\Phi_n^{\mathrm{T}}(I - K_{n+1}H_{n+1})^{\mathrm{T}}. \qquad (4.63)
\end{aligned}$$

By setting Eq.(4.59) and Eq.(4.63) equal, one can obtain

$$E\{v_n^{(2)}v_{n+1}^{(2)\mathrm{T}}\} = P_{\hat{x}_n^+}\Phi_n^{\mathrm{T}}(I - K_{n+1}H_{n+1})^{\mathrm{T}}. \qquad (4.64)$$

Combining Eq.(4.60) ,Eq.(4.61) and Eq.(4.64), Γ_n can be computed as

$$\begin{aligned}
\Gamma_n &= (E\{v_n^{(2)}v_{n+1}^{(2)\mathrm{T}}\})^{\mathrm{T}}((E\{v_n^{(2)}v_n^{(2)\mathrm{T}}\})^{\mathrm{T}})^{-1} \\
&= (I - K_{n+1}H_{n+1})\Phi_n P_{\hat{x}_n^+}^{\mathrm{T}}(P_{\hat{x}_n^+}^{\mathrm{T}})^{-1} \\
&= (I - K_{n+1}H_{n+1})\Phi_n. \qquad (4.65)
\end{aligned}$$

This last equation shows the existence of a time-correlation between state estimates at the output of a Kalman Filter. If there was no correlation, the Γ_n would be equal to zero to match the standard Kalman filter model. However, it would mean that the matrix product K_nH_n is equal to the identity matrix, which is very unlikely considering the form of K_n. This validate the need of the Bryson method in the second stage in order to take this correlation into account.

4.3.3 Second Stage

The second stage Kalman Filter focuses on computing an estimate of $\Delta\tilde{g}$ defined as in (4.49). The second state vector is defined as follows:

$$x^{(2)} = \left[\Delta\vec{r}^{K,\mathrm{T}}, \Delta\dot{\vec{r}}^{K,\mathrm{T}}, c\delta\tau_R^{\mathrm{T}}, b_{g^K}^{\mathrm{T}}\right]^{\mathrm{T}}. \qquad (4.66)$$

It is noted that the receiver clock offset term $c\delta\tau_R$ also contains the receiver code bias, which cannot be distinguished from the clock offset.

The orbital error $\Delta\vec{r}^K$ has a linear state model:

$$\Delta\vec{r}^K(t_n) = \Delta\vec{r}^K(t_{n-1}) + \Delta t\Delta\dot{\vec{r}}^K(t_{n-1}) + w_{\Delta\vec{r}^K}(t_n). \qquad (4.67)$$

The estimate $\Delta\hat{\tilde{g}}$ from the first Kalman filter serves as the measurement input for the second one.

$$z^{(2)} = \Delta\hat{\tilde{g}}. \qquad (4.68)$$

Similar with the first stage, the state transition matrix can be derived from the dynamical model of (4.67):

$$\Phi_n = \begin{pmatrix} \mathbb{1} & \Delta t\mathbb{1} & 0 & 0 \\ 0 & \mathbb{1} & 0 & 0 \\ 0 & 0 & \mathbb{1} & 0 \\ 0 & 0 & 0 & \mathbb{1} \end{pmatrix}. \tag{4.69}$$

Equation (4.49) gives directly the form of the H_n matrix:

$$H_n = \begin{pmatrix} H_{\Delta\vec{r}} & 0 & H_{c\delta\tau_R} & H_{b_{g^K}} \end{pmatrix}, \tag{4.70}$$

with

$$H_{c\delta\tau_R} = \begin{pmatrix} \mathbb{1}^{K_1\times 1} & & & \\ & \mathbb{1}^{K_2\times 1} & & \\ & & \ddots & \\ & & & \mathbb{1}^{K_R\times 1} \end{pmatrix}. \tag{4.71}$$

The matrix $H_{\Delta\vec{r}}$ contains the $\vec{e}$-vectors for each satellite/receiver pair. Since the radial component of the orbital error is the most difficult term to be estimated during a short time, it is necessary to separate the radial direction from the normal e-vector. In this work, the RIC (Radial, In-track, and Cross-track) frame is used to describe the orbital error, and the transformation matrix into ECEF (Earth Centered Earth Fixed) frame [16] is explained in the following.

Consider a coordinate (X, Y, Z) in the ECI (Earth-Centered Inertial) frame, the radius, velocity and angular momentum are then obtained as

$$\vec{r} = X\vec{e}_{x,\mathrm{I}} + Y\vec{e}_{y,\mathrm{I}} + Z\vec{e}_{z,\mathrm{I}} \tag{4.72}$$

$$\dot{\vec{r}} = \dot{X}\vec{e}_{x,\mathrm{I}} + \dot{Y}\vec{e}_{y,\mathrm{I}} + \dot{Z}\vec{e}_{z,\mathrm{I}} \tag{4.73}$$

$$\vec{L} = \vec{r} \wedge \dot{\vec{r}}, \tag{4.74}$$

with

$\vec{r}$	:	position vector
$(\vec{e}_{x,\mathrm{I}}, \vec{e}_{y,\mathrm{I}}, \vec{e}_{z,\mathrm{I}})$	:	triplet of the ECI frame
$\dot{\vec{r}}$	:	velocity vector
$\vec{L}$	:	angular momentum vector

The three base axis of the RIC frame are $\vec{R}$ lies along the instantaneous radius vector, $\vec{C}$ lies along the angular momentum vector, and $\vec{I}$ completes the right hand system, i.e.

$$\vec{R} = \frac{\vec{r}}{\|\vec{r}\|} = \frac{X}{\|\vec{r}\|}\vec{e}_{x,\mathrm{I}} + \frac{Y}{\|\vec{r}\|}\vec{e}_{y,\mathrm{I}} + \frac{Z}{\|\vec{r}\|}\vec{e}_{z,\mathrm{I}} \tag{4.75}$$

$$\vec{C} = \frac{\vec{L}}{\left\|\vec{L}\right\|} = \frac{\vec{r} \wedge \dot{\vec{r}}}{\left\|\vec{r} \wedge \dot{\vec{r}}\right\|} \tag{4.76}$$

$$\vec{I} = \vec{C} \wedge \vec{R}. \tag{4.77}$$

Therefore the rotation matrix from ECI to RIC is defined as

$$\begin{pmatrix} \vec{R} \\ \vec{I} \\ \vec{C} \end{pmatrix} = \begin{pmatrix} R_x & R_y & R_z \\ I_x & I_y & I_z \\ C_x & C_y & C_z \end{pmatrix} \begin{pmatrix} \vec{e}_{x,\mathrm{I}} \\ \vec{e}_{y,\mathrm{I}} \\ \vec{e}_{z,\mathrm{I}} \end{pmatrix}$$
$$= R_{\mathrm{RIC}} \begin{pmatrix} \vec{e}_{x,\mathrm{I}} \\ \vec{e}_{y,\mathrm{I}} \\ \vec{e}_{z,\mathrm{I}} \end{pmatrix}. \tag{4.78}$$

To perform the change of coordinates from ECI to ECEF, the rotation of the earth of an angle θ between the two frames must be taken into account. The rotation matrix $R_z(\theta)$ along the z axis is given by

$$\begin{pmatrix} \vec{e}_x \\ \vec{e}_y \\ \vec{e}_z \end{pmatrix} = \begin{pmatrix} \cos(\theta) & \sin(\theta) & 0 \\ -\sin(\theta) & \cos(\theta) & 0 \\ 0 & 0 & 1 \end{pmatrix} \cdot \begin{pmatrix} \vec{e}_{x,\mathrm{I}} \\ \vec{e}_{y,\mathrm{I}} \\ \vec{e}_{z,\mathrm{I}} \end{pmatrix}$$
$$= R_z(\theta) \cdot \begin{pmatrix} \vec{e}_{x,\mathrm{I}} \\ \vec{e}_{y,\mathrm{I}} \\ \vec{e}_{z,\mathrm{I}} \end{pmatrix}. \tag{4.79}$$

The final transformation from RIC to ECEF can be described as:

$$\begin{pmatrix} \Delta r_x \\ \Delta r_y \\ \Delta r_z \end{pmatrix} = R_z(\theta) \cdot R_{\mathrm{RIC}}^{\mathrm{T}} \begin{pmatrix} \Delta r_{\mathrm{R}} \\ \Delta r_{\mathrm{I}} \\ \Delta r_{\mathrm{C}} \end{pmatrix}. \tag{4.80}$$

4.4 Results

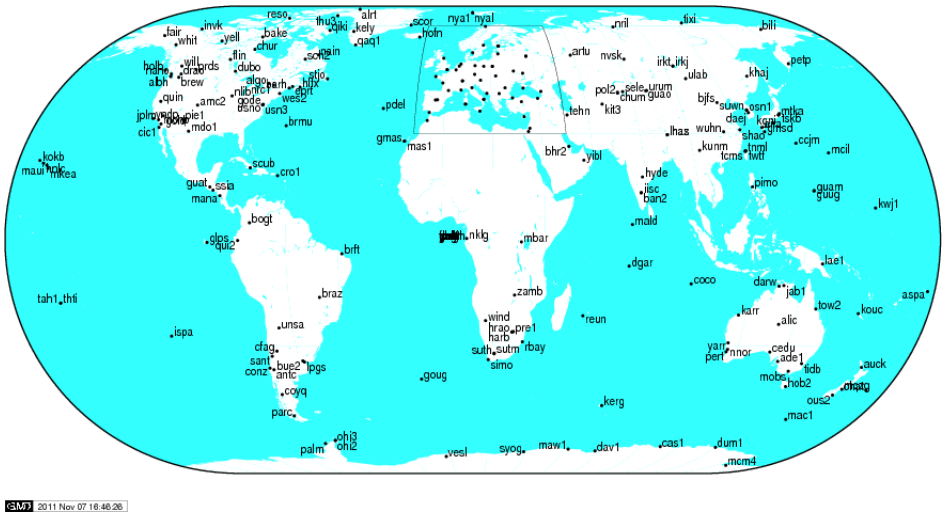

Figure 4.1: IGS global network of stations used in the simulation

In this work, a simulation based on a network of receivers worldwide [6] is performed to estimate the satellite orbital errors and satellite code biases

along with other terms. In the simulation step, the state including the satellite orbital errors, the receiver clock offsets, the satellite code biases, the ionospheric slant delays, the integer ambiguities, the receiver and satellite phase biases is generated in one step, which is further estimated using the cascaded Kalman filter. The geometry term is estimated in the first Kalman filter, and then used as measurement in the second Kalman filter. The Bryson method is applied to decouple the time-correlated measurements.

The generated satellite orbital error consists of the in-track and along-track components, where the radial component is assumed to be perfectly known. Signals were generated without multipath and the ambiguities are fixed. Fig.4.2 shows the difference between the true orbital errors and the estimates. The error in the estimates converges to under 2 cm after 700 epochs. Fig.4.3 shows the error in the satellite code bias estimates. After 500 epochs the error converges to under 1 cm.

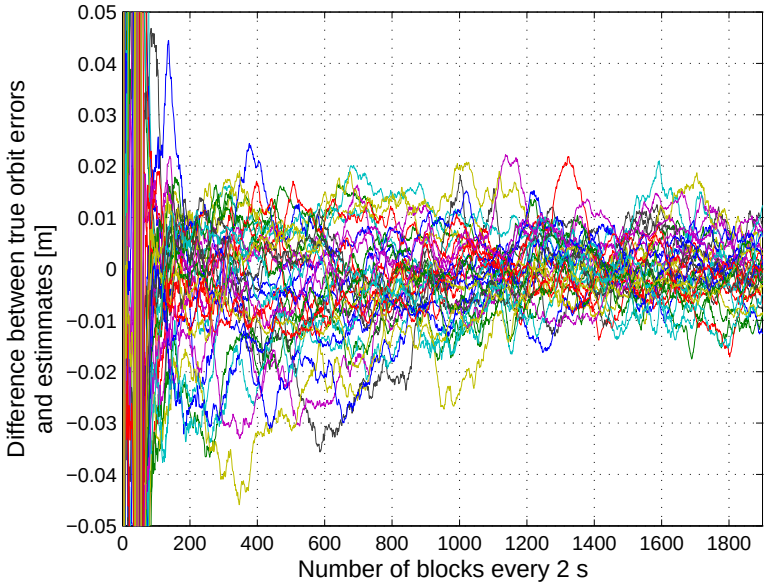

Figure 4.2: Difference between true orbital errors and estimates for in-track and along-track

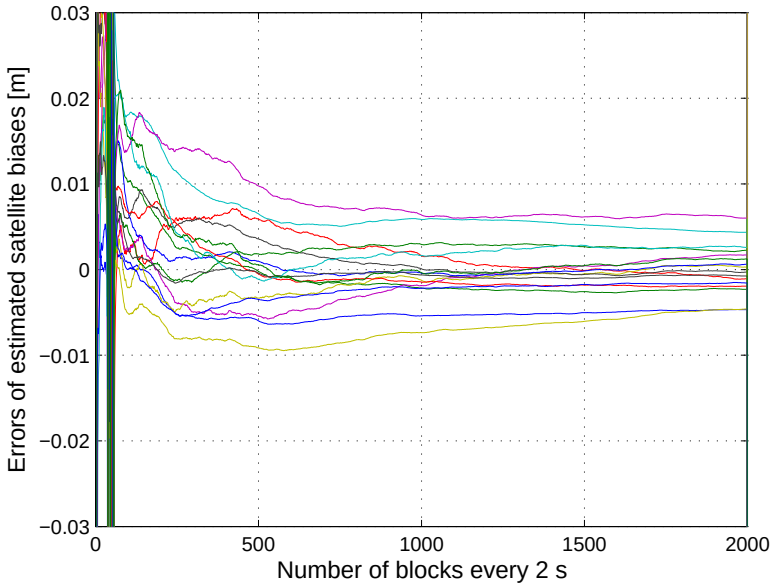

Figure 4.3: Difference between true geometry satellite code biases and estimates

Chapter 5

Multipath Correction

5.1 Presentation of the SAPOS Network

This chapter focuses on the reduction of code multipath. Real GPS data were obtained from the *Satellitenpositionierungsdienst der deutschen Landesvermessung* (SAPOS), which operates a network of geodetic reference stations in Bavaria.

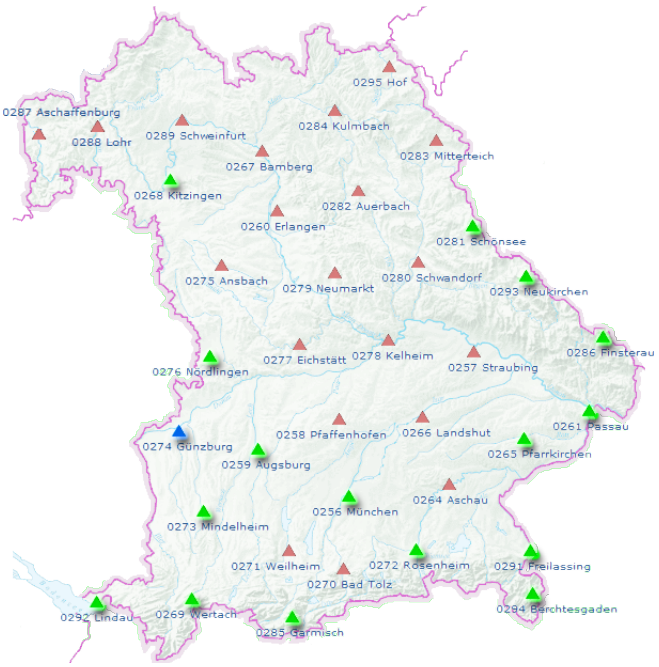

Figure 5.1: SAPOS network in Bavaria

Fig.5.1 shows a map of the whole Bavarian network of SAPOS stations [17]. The stations used in the simulation are marked green and use common Trimble receivers. The data were taken over 7 days from Mai 30, 2011 to June 5, 2011 during the period 8:00 - 11:00 local time (UTC+2). A subset of 10 stations were

chosen, with the following computation parameters for the process noises:

$$\begin{aligned} \sigma_{w_{g_i}} &= 1 \text{ m} \\ \sigma_{w_I} &= 1 \text{ cm} \\ \sigma_{w_{\beta_i}} &= \sigma_{w_{\beta^k}} = \sigma_{w_N} = 0, \end{aligned}$$

with $\sigma_{w_{g_i}}$, σ_{w_I}, $\sigma_{w_{\beta_i}}$, $\sigma_{w_{\beta^k}}$, σ_{w_N} being respectively the process noise standard deviation for the geometry term, the ionospheric delay, the receiver and satellite biases and the ambiguities. The satellites considered are those seen by all stations during the 3 hour time period and are the following: PRN2, PRN5, PRN7, PRN8, PRN10 and PRN13. The stations presenting the most interesting results is the 0274 in Günzburg marked with a blue triangle on the map 5.1.

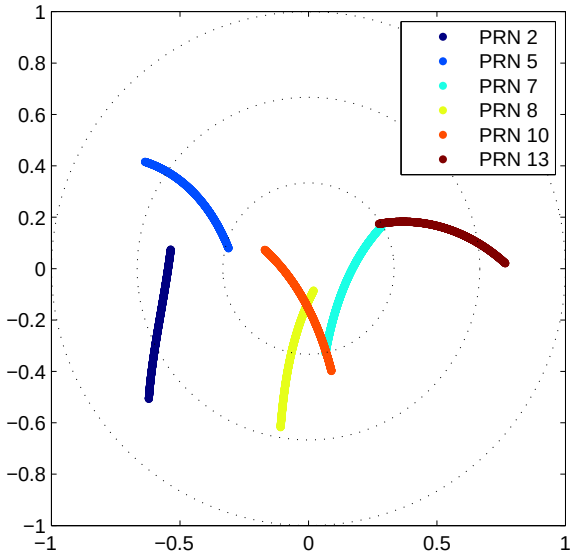

Figure 5.2: Skyplot of the station 0274

The Figure 5.2 shows the skyplot of the station 0274 and the 6 chosen satellites during the observation period. It is a polar representation of the satellite position seen by a receiver. The angle is equal to the azimuth and the radius is equal to the satellite elevation in the sky. Most of the patterns studied in the following come from the PRN5 represented with the blue curve located in the upper left corner.

5.2 Multipath Analysis

In a perfectly modeled system the residual of the code and phase should be almost equivalent to a white gaussian noise. However, the residual (Fig.5.3) over time shows that there exists a strong periodic pattern, which is most likely to be the code multipath.

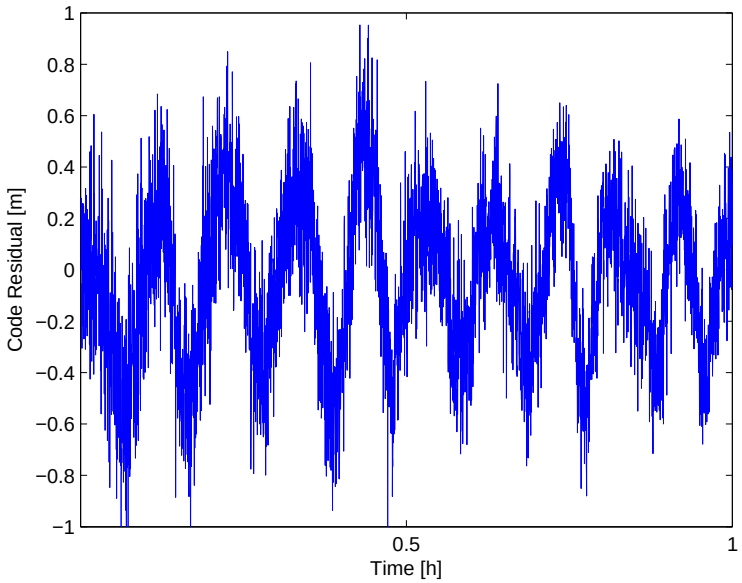

Figure 5.3: Residual of pseudorange measurements at station 0274 from PRN5 on days 150 from 8:00 to 9:40.

The pattern also repeats itself after a GPS period as seen on Fig.5.4 and the magnitude of the oscillation seems directly correlated to the current satellite elevation and thus position toward the station and its environment, being almost nonexistent for high elevation.

Using the cross-correlation function $*$, this phenomenon can be understood easily. The cross-correlation between two signal f and g is a measure of similarity of the two waveforms. It allows pattern recognition by making the convolution between the two signals without reversing and is defined as

$$(f * g)[m] = \sum_{n=-\infty}^{\infty} f^*[m]g[n+m]. \tag{5.1}$$

Fig.5.5 represents the cross-correlation figure of two stations between 2 days. On Figure 5.5(a), the normalized cross-correlation result shows a characteristical sinc looking aspect with a maximum at time $t_n = 3$ min 56 s (difference between the time period between the two sample, which is a calendar day, and a sidereal day, which is equal to 2 periods of GPS). Furthermore, the side lobes have a constant spacing corresponding to the time period of the oscillating pattern. On Figure 5.5(b), there is no clear maximum that can be sorted out and the normalized cross-correlation result includes significant noise, proving that there is no real pattern to be matched between the two samples. Moreover, the maximum in the second case is ten times lower than the maximum in the first case. This can be explained by multipath occurring at low elevation: the signal from the satellite is bouncing on the surrounding environment of the base antenna, creating destructive and constructive interferences and thus producing the same pattern each time the satellite is in sight. It means that every

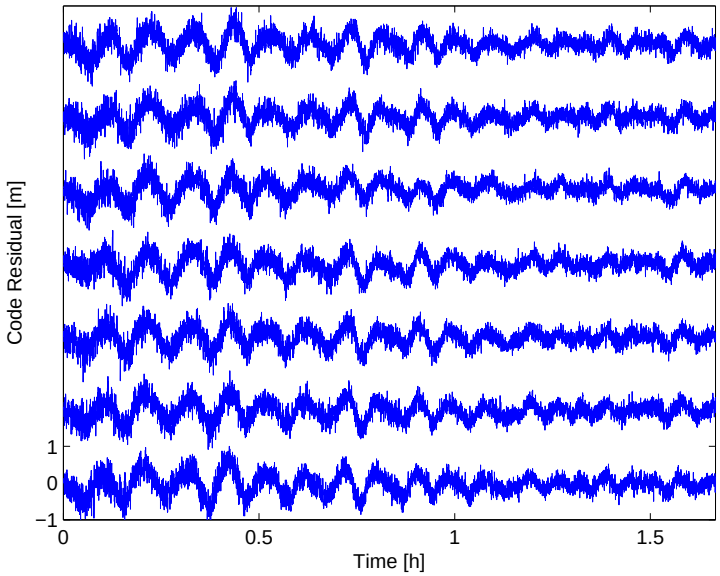

Figure 5.4: Residual of pseudorange measurements at station 0274 from PRN5 on days 150 to 156 from 8:00 to 9:40.

11h58m02s (1 GPS revolution period) the residual has the same aspect in case of strong multipath/shadowing. The residual res can be described as

$$res = z - H\hat{x}^+ = m + \eta, \tag{5.2}$$

with z being the measurement, $\hat{x}^+$ the state estimate, H the measurement matrix, m the multipath term and η a white gaussian noise. In order to get the multipath pattern, a simple method consists in averaging n samples of the residual in order to obtain the estimate as

$$\hat{m} = m + \frac{1}{n}\eta. \tag{5.3}$$

If the noise η has a variance σ^2, the 'new' noise component of $\hat{m}$ has a variance of $\frac{\sigma^2}{n}$ (The family of normal distributions is closed under linear transformations and the linear combination of independent normal random variables is also normally distributed). It means that the more samples are used, the less noisy the estimated pattern will be as seen on Fig.5.6, where the residuals from Fig.5.4 have been averaged in respect to their elevation.

5.3 Multipath Correction on the Residuals

To apply the correction, the multipath amplitude of the average is subtracted to the code and phase measurement elevation-wise with respect to the rising and setting of the satellite (see (5.4)). The effect on the residual is the disappearance

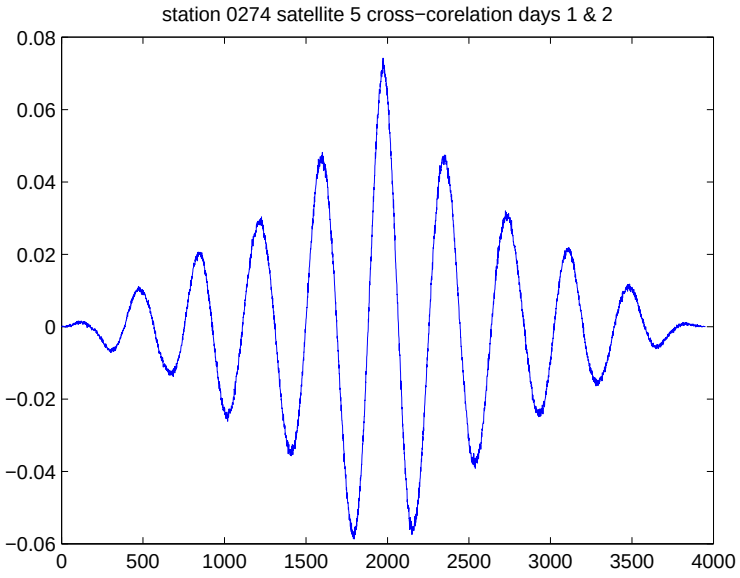

(a) High correlation

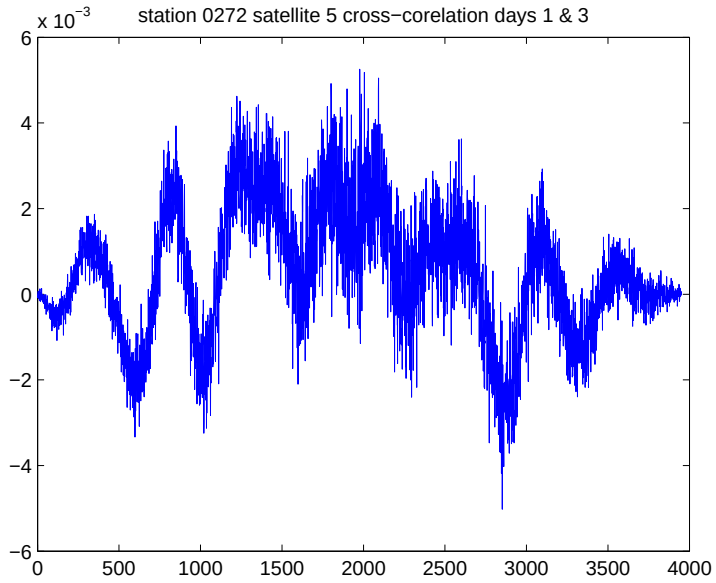

(b) low Correlation

Figure 5.5: Cross-correlation figure of two samples from different days at the same daily hour

of the multipath pattern which can be seen on Fig.5.7.

$$z_{\text{new}} = z - \hat{m}. \tag{5.4}$$

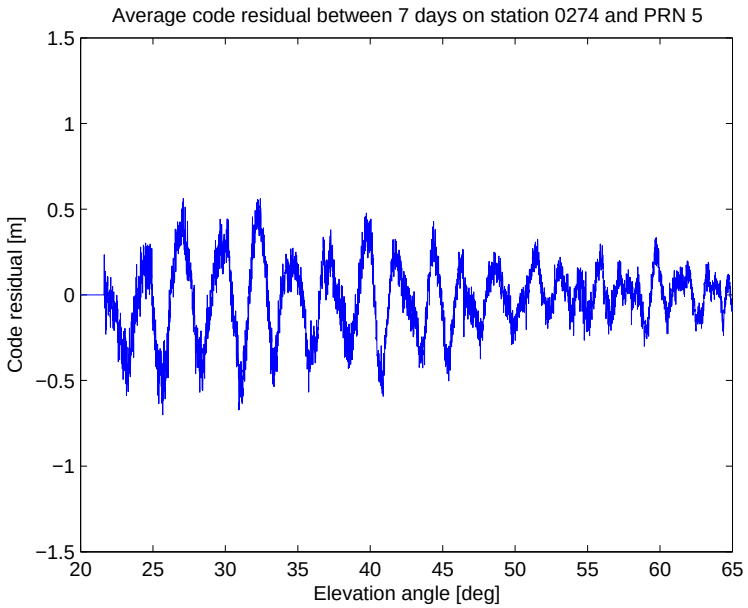

Figure 5.6: Averaging over one week

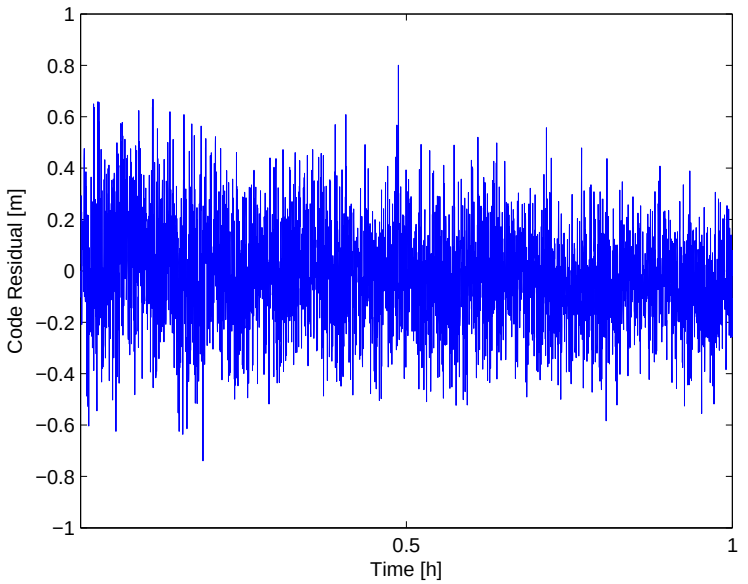

Figure 5.7: Code residual for station 0274 PRN 5 on day 150 after the application of the multipath filtering

$$res = \frac{n+1}{n}\eta. \tag{5.5}$$

Spectral analysis can also bring some information about the nature of the residual. One way of obtaining the spectral density of a signal is the use of a periodogram which provide an estimate of it. In a time-discrete model, the FFT (fast Fourier transform) is used to allow the access of such a periodogram. Let $x_0, \ldots, x_{N-1}$ be complex number defining the time-discrete signal, with N being a power of 2. The DFT (discrete Fourier Transform) which serves as a base for the FFT is described as

$$X_k = \sum_{n=0}^{N-1} x_n e^{i2\pi k \frac{n}{N}}, \tag{5.6}$$

with $k = 0, \ldots, N-1$

The power of the FFT, i.e. the periodogram is then computed as

$$\text{Periodogram}_k = \frac{1}{N} X_k * X_k^*, \tag{5.7}$$

with X_k^* being the conjugate of X_k.

Applied to the residual, a rough estimate of the spectral density is obtain on Fig.5.8.

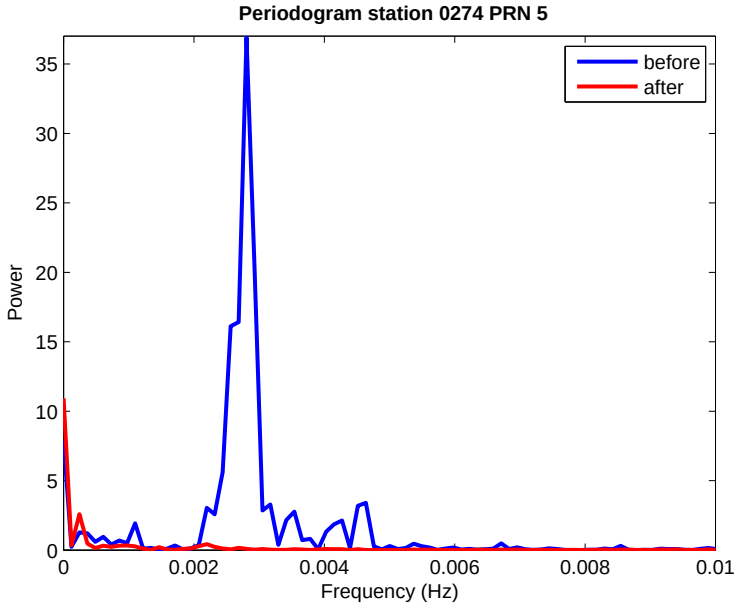

Figure 5.8: Periodogram of 0274 PRN 5

In the case of an ideal white Gaussian noise, the power shall remain constant in respect to the frequency. Peaks are to be noted at the frequencies corresponding on the oscillations of the pattern in case of multipath (blue curve). Those

peaks get completely discarded when the multipath correction is applied (red curve) giving the residual a closer aspect to white noise. On Fig.5.9, the histogram of the residual before and after correction has been plotted. It has a typical bell-shape of a Gaussian noise in both cases.

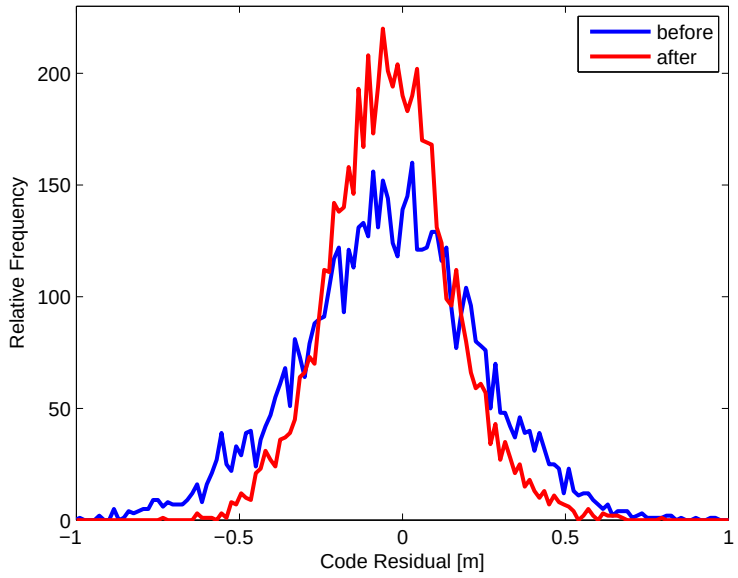

Figure 5.9: Distribution of the residual for station 0274 PRN 5

It can be seen that the blue curve is much wider aspect than the red curve, which translates by a greater variance of the signal. After measurement, the corrected residual presents a variance reduced by a factor 2 compared to the original uncorrected residual.

5.4 Results

The direct effect of multipath correction on the satellite phase bias estimation is the improved stability as seen on Fig.5.10. The erratic oscillations are discarded and the curves converge smoothly to their final values.

The vertical black bars of Fig.5.10 denote ambiguities fixing. Before the multipath correction, only 2 out of 90 ambiguities were fixed over a period of 6000 s. With multipath correction, this number is raised to 40 out of 90 for this particular set of data. Moreover the fixing of the first ambiguity happens earlier: without multipath correction the first fixing occurs at $t = 3668$ s, whereas the first fixing with multipath correction occurs at $t = 2219$ s.

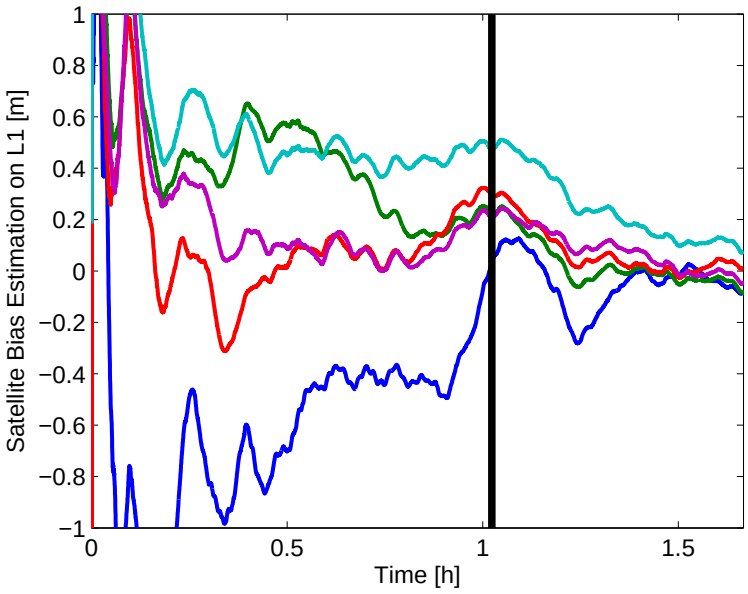

(a) before

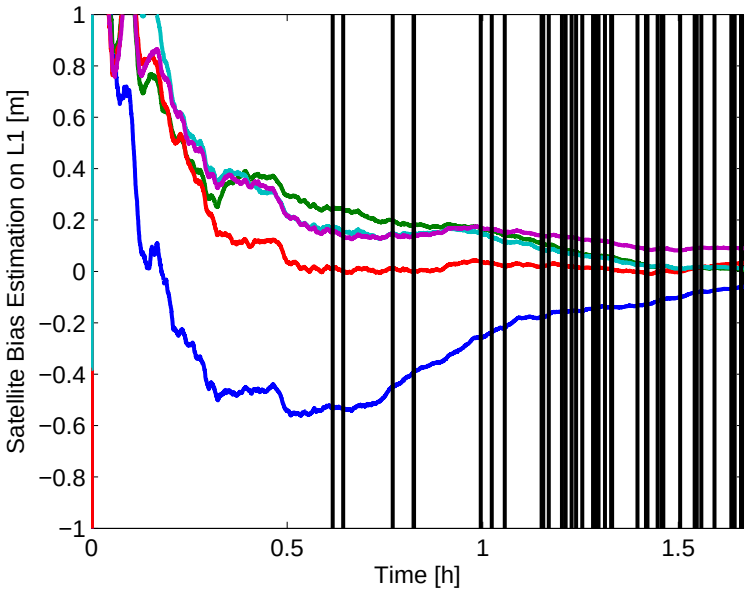

(b) after

Figure 5.10: Phase bias estimate on the L1 frequency

Chapter 6

Conclusion

In this work, a cascaded Kalman filter was developed to estimate satellite phase and code biases in a GNSS network. First, a set of mappings has been performed on the most general measurement model to prevent singularities. A first stage Kalman filter has then been applied to this model in order to retrieve an estimate of the geometry term containing all non-dispersive parameters. After this step, a second Kalman filter has been used to refine this geometry term or, more precisely, to determine satellite orbit corrections and satellite code biases. As the a posteriori state estimates of the first Kalman filter correspond to the measurements of the second Kalman filter, the time-correlation introduced by the first Kalman filter has been taken into account by Bryson's generalized Kalman filter for coloured measurement noises. A decoupling has been performed in two steps - the first one being a time-differencing and the second one being a decorrelation of the transformed measurement and process noises.

A simulation based on a network of receivers from IGS has been performed to estimate the satellite cross-track and in-track orbital errors as well as satellite code biases along with other terms. The difference between the estimated orbital errors and their true values converges to less than 2 cm within 1400 s. For the satellite code biases estimate, this difference reaches 1 cm after 1000 s.

The second part of the thesis focused on the mitigation of code multipath. Given a network of ground station from SAPOS split across Bavaria, a daily multipath pattern has been observed in the code measurements. A sidereal filtering has been applied to the samples gathered over one week, such that the multipath pattern could be isolated and removed from the measurements. The effect on real data was an almost complete mitigation of the pattern, resulting in an almost white measurement noise and in an increase of the ambiguity fixing from 2.22 % to 44.44 % of the total ambiguities for the observed time period. The fixing of the ambiguities also happens earlier when the multipath is corrected, thus providing a faster estimation of the phase biases.

Bibliography

[1] D. Laurichesse and F. Mercier, "Integer ambiguity resolution on undifferenced gps phase measurements and its application to ppp." Proc. of ION-GNSS, Forth Worth, USA, pp. 839-848, Sept. 2007.

[2] D. Laurichesse, F. Mercier, J.-P. Berthias, P. Brocca, and L. Cerri, "Integer ambiguity resolution on undifferenced gps phase measurements and its application to ppp and satellite precise orbit determination." Navigation, Vol. 56, No. 2, pp. 135-149, 2009.

[3] D. Laurichesse, F. Mercier, and J.-P. Berthias, "Real-time ppp with undifferenced integer ambiguity resolution, experimental results." Proc. of 23rd ION Intern. Techn. Meet. (ION-GNSS), pp. 2534-2544, Portland, USA, Sept. 2010.

[4] G. Wübbena, "GPS carrier phases and clock modeling." Lecture Notes in Earth Sciences: GPS-Techniques Applied to Geodesy and Surveying, vol. 19, pp. 381-392, 1988.

[5] K. Wang, Y. Li, and C. Rizos, "A new practical approach to kalman filtering with time-correlated measurement errors," 2010.

[6] "International GNSS service website." http://igscb.jpl.nasa.gov, Sept. 2011.

[7] P. Henkel, Z. Wen, and C. Günther, "Estimation of code and phase biases on multiple frequencies with a kalman filter." Proc. of 4-th European Workshop on GNSS Signals and Signal Processing, Oberpfaffenhofen, Germany, Dec. 2009.

[8] P. Henkel, Z. Wen, and C. Günther, "Estimation of satellite and receiver biases on multiple galileo frequencies with a kalman filter." Proc. of ION Int. Techn. Meeting, ION, San Diego, USA, 2010.

[9] Z. Wen, P. Henkel, and C. Günther, "Reliable estimation of phase biases of gps satellites with a local reference network." Proc. of 53rd IEEE Intern. Symposium ELMAR, Zadar, Croatia, pp. 321-324, Sept. 2011.

[10] C. Günther, "Satellite navigation." Lecture notes, Technische Universität München, 2011.

[11] Z. Wen, "Estimation of code and phase biases in satellite navigation." Master Thesis, Technische Universität München, Mai 2010.

[12] R. Brown and P. Hwang, "Introduction to random signals and applied kalman filtering." 3rd edition, John Wiley & Sons, New York, 1997.

[13] A. J. Bryson and L. Henrikson, "Estimation using sampled data containing sequentially correlated noise." Journal of Spacecraft and Rockets, 5(6), 662-665, 1968.

[14] P. Henkel, "Reliable carrier phase positioning with multiple frequencies." Phd Thesis, Technische Universität München, 2010.

[15] P. Henkel, "Precise Point Positioning with GPS and Galileo." lecture notes, 2011.

[16] G. Born, "Introduction to statistical orbit determination." Lecture notes, University of Colorado.

[17] "Sapos Bayern - Referenzstationen." http://sapos.bayern.de, Sept. 2011.